Ore Geology Reviews 88 (2017) 251–269

Contents lists available at ScienceDirect

Ore Geology Reviews

journal homepage: www.elsevier.com/locate/oregeo

Early Cretaceous high-Mg adakites associated with Cu-Au mineralization in the Cebu Island, Central Philippines: Implication for partial melting of the paleo-Pacific Plate

Jianghong Deng [a], Xiaoyong Yang [a,*], Huasheng Qi [a], Zhao-feng Zhang [b], Abdul Shakoor Mastoi [a], Weidong Sun [c,d,e,*]

[a] CAS Key Laboratory of Crust-Mantle Materials and Environments, University of Science and Technology of China, Hefei 230026, China
[b] State Key Laboratory of Isotope Geochemistry, Guangzhou Institute of Geochemistry, Chinese Academy of Sciences, Guangzhou 510640, China
[c] Center of Deep Sea Research, Institute of Oceanology, Chinese Academy of Sciences, Qingdao 266071, China
[d] Laboratory for Marine Mineral Resources, Qingdao National Laboratory for Marine Science and Technology, Qingdao 266237, China
[e] CAS Center for Excellence in Tibetan Plateau Earth Sciences, Chinese Academy of Sciences, Beijing 100101, China

ARTICLE INFO

Article history:
Received 21 December 2016
Received in revised form 3 May 2017
Accepted 8 May 2017
Available online 11 May 2017

Keywords:
Adakite
Slab melting
Porphyry Cu deposit
Paleo-Pacific Plate subduction
Cebu Island
Central Philippines

ABSTRACT

Early Cretaceous arc volcanic rocks, diorite intrusions and an associated large porphyry deposit occur in the Cebu Island, Central Philippines. In this paper, we studied the diorite porphyries associated with Cu-Au mineralization in the Kansi region, where Early Cretaceous arc volcanic rocks are widely distributed. Zircon U-Pb age reveals that the diorites were formed at ca. 110 Ma, close to the formation age of Lutopan diorites in the famous Atlas porphyry Cu-Au deposit (109–101 Ma), and younger than those of the arc volcanics in this region (126–118 Ma). The Kansi diorites and Lutopan diorites are both calc-alkaline high-Mg adakites with high Sr/Y ratios. Their major elements define similar variation trends in Harker diagrams, suggesting that they were probably generated from a uniform source but experienced different degree of partial melting or fractional crystallization. The Kansi diorites are characterized by LREE enrichment, HREE depletion, no Eu negative anomaly, with enrichment of Pb, Sr, Zr and Hf and depletion of Nb, Ta, and Ti. They are probably generated by the partial melting of subducted oceanic crust, followed by a certain degree of mantle interaction and crustal contamination. The highly depleted Sr-Nd-Pb-Hf isotopes of the Kansi diorites are close to the Amami Plateau basalt and tonalite, indicating the dominance of a Pacific-type MORB in the source. The Cu-Au mineralization-related Kansi diorites are characterized by high oxygen fugacities more than ΔFMQ +2, indicating quite a good potential for porphyry Cu-Au mineralization in the region. Finally, in our tectonic model, the successive generation of arc volcanic rocks and adakites in the Cebu Island are responses to the subduction and rollback of the paleo-Pacific Plate to the proto-Philippine Sea Plate (PSP) in the Early Cretaceous.

1. Introduction

Adakites have been originally proposed to be generated by partial melting of hot and young (≤25 Ma) subducting oceanic crust at convergent margin according to Defant and Drummond (1990). They are intermediate-felsic, usually amphibole-rich volcanic or plutonic rocks displaying high Sr and La, but low Y and Yb signatures that result in high Sr/Y and La/Yb ratios. Adakites are not only found in the tectonic settings of forearc region, main volcanic arc, back-arc (Castillo, 2012; Defant and Drummond, 1990; Drummond et al., 1996), with subducting oceanic crust as a necessary component, but also in intraplate regions, where partial melting of thickened or delaminated continental crust happened (Chiaradia et al., 2009; Chung et al., 2003; Wang et al., 2007). They may have high MgO contents and Mg#, high Cr, Ni contents, reflecting interaction between pristine slab melts and mantle peridotite (Defant and Drummond, 1990; Defant and Kepezhinskas, 2001; Martin et al., 2005; Stern and Kilian, 1996). Adakites are usually closely associated with large gold-bearing porphyry copper deposits and related epithermal vein systems (Oyarzun et al., 2001; Sajona and Maury, 1998; Sun et al., 2010, 2012, 2015; Thieblemont et al., 1997; Zhang et al., 2004).

* Corresponding authors at: CAS Key Laboratory of Crust-Mantle Materials and Environments, University of Science and Technology of China, Hefei 230026, China (X. Yang); Center of Deep Sea Research, Institute of Oceanology, Chinese Academy of Sciences, Qingdao 266071, China (W. Sun).
E-mail addresses: xyyang555@163.com (X. Yang), weidongsun@gig.ac.cn (W. Sun).

http://dx.doi.org/10.1016/j.oregeorev.2017.05.006
0169-1368/

The Philippine island arc system, located at the boundary of the Eurasian and West Philippine Sea Plate (PSP), is a collage of amalgamated terranes of oceanic, continental and island arc affinities (e.g., Faure et al., 1989; Yumul et al., 1997), providing an ideal setting to investigate the tectono-magmatic processes in a convergent margin. Volcanic activities and igneous intrusions have been active since the Cretaceous as suggested by the presence of magmatic belts of Cretaceous to Quaternary ages. Most of them are related to subduction events, with a prominent peak in the Eocene (e.g., formation of the Sierra Madre Mountains of northern and central Luzon), Middle Miocene (e.g., formation of the Cordillera mountains in northern Luzon) and Plio-Quaternary (Recent volcanic arc) (Aurelio et al., 2013), triggering the wide development of Cenozoic arc volcanic rocks, Nb-enriched basalt, adakites and large Cu-Au deposits (e.g., Castillo et al., 1999, 2007; Jego et al., 2005; Sajona et al., 1996; Yumul et al., 2000b). Cenozoic adakites in the Philippines are widely studied, and there are several genetic models for these adakites in different areas: e.g., partial melting of the subducted South China Sea Plate with reaction of the island arc mantle wedge for the Bataan Island adakites, Northern Luzon arc (Schiano et al., 1995; Zhan et al., 2015); partial melting of the lower arc crust for the adakites from Northern and Central Luzon (Bellon and Yumul, 2001; Yumul et al., 2000a; Yumul et al., 2003); low (<10%) degree of partial melting of young subducted Sulu Sea slab in garnet amphibolite facies for the Negros adakites, Central Philippines (Sajona et al., 2000a); slab melting (Sajona et al., 1993) or fractionation of mantle derived basaltic arc magmas (Castillo et al., 1999; Macpherson et al., 2006; Yumul et al., 2016) for the Camiguin and Mindanao adakites; and mixing of adakitic and mantle-derived mafic magmas (Jego et al., 2005).

In contrast, adakites with Early Cretaceous ages have been rarely reported in the Philippines. In this study, we report Early Cretaceous adakites which are related to Cu-Au mineralization in the Cebu Island. Based on comprehensive geochronological and geochemical studies, and the tectonic evolution of the Pacific Plate, this study is aiming to reveal their petrogenesis and magma sources, and discuss their tectonic environment by combining them with Early Cretaceous arc volcanics in the area. We also compare them with the Lutopan Diorite in the Atlas porphyry Cu-Au deposit (the only Early Cretaceous large porphyry Cu-Au deposit so far discovered in the Philippine Islands) in the Cebu Island, to discuss their potential for large porphyry Cu-Au mineralization.

2. Regional geology and sample description

The Philippine region is a collage of amalgamated terranes of oceanic, continental and island arc affinities, constituting the Palawan micro-continental block and the seismically-active Philippine Mobile Belt (PMB), which are characterized by strong seismicity and active volcanoes (Walia et al., 2012; Yumul, 2007; Yumul et al., 2008). The PMB or the Philippine archipelago is bounded by subduction zones to the east and west. The eastward subduction of the Early Oligocene to Early Miocene South China Sea plate, the Early to Middle Miocene Sulu Sea plate, and the Eocene Celebes basin plate formed the Manila Trench, Negros and Sulu Trenches, and Cotabato Trench in the western boundary, respectively (Fig. 1a) (e.g. Mitchell et al., 1986; Rangin et al., 1999). On the eastern boundary of the archipelago, the westward oblique subduction of Eocene West PSP formed the East Luzon Trough-Philippine Trench (Ozawa et al., 2004). The Indo-Australian plate is in the south of the archipelago. The Pliocene-aged sinistral strike-slip Philippine Fault Zone (PFZ), which is a product of shear partitioning due to the oblique convergence of the PSP and the Sundaland/Eurasian Plate (e.g., Aurelio, 2000; Aurelio et al., 2013; Quebral et al., 1996), longitudinally cut through the archipelago (Fig. 1a).

Central Philippines which is bound by the east-dipping Negros Trench in the west and the west-dipping Philippine Trench in the east, comprise the islands of Panay, Negros, Cebu, Bohol, Leyte, Samar and Masbate, being cut by the PFZ through Leyte and

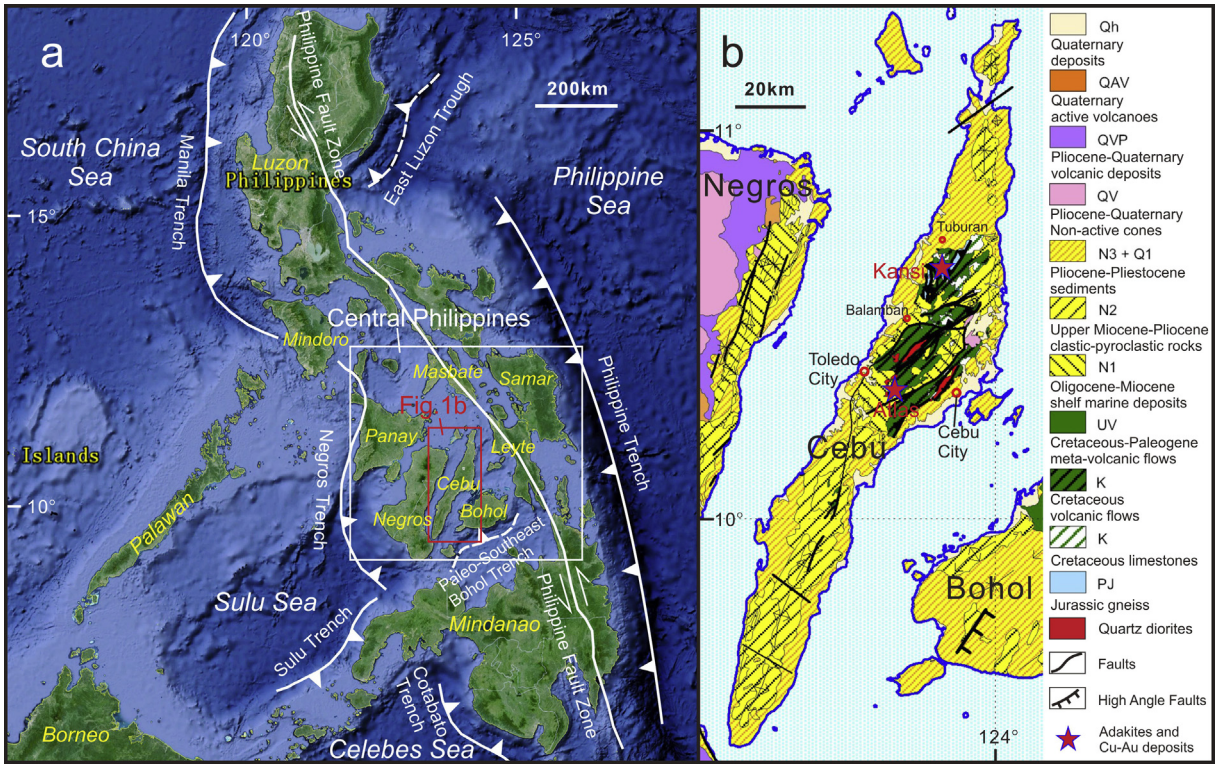

Fig. 1. Sketch map showing geological settings of the Philippine archipelago (a), and geological map of the Cebu Island (b). After Google Earth and Aurelio and Peña (2010).

Masbate (Fig. 1a). The basement of Central Philippines is composed of complete to dismembered crust-mantle sequence ophiolite complexes with regional metamorphic rocks and intrusive/extrusive igneous complexes, in age ranging from Cretaceous to Eocene. These ophiolite complexes contain rocks with transitional mid-ocean ridge basalt (MORB) and island arc tholeiite (IAT) geochemical signatures (Dimalanta and Yumul, 2006; Yumul, 2007). Some of the ophiolites or ophiolitic complexes host metallic mineral deposits such as chromite, nickel, platinum-group minerals and massive sulfides (Dimalanta et al., 2006; Tamayo et al., 2001).

The basement complexes of Cebu Island comprise dismembered lherzolites and harzburgites, Jurassic metamorphic rocks, Cretaceous volcanic rocks and a sedimentary unit (Dimalanta et al., 2006), which are mostly exposed in the central part of the island (Fig. 1b). The Jurassic Tunlob Schist which is the oldest rock in the island, is composed of albite-epidote-amphibolite facies chloritic orthoschist and micaceous paraschist (Aurelio and Peña, 2002). They are unconformably overlain by the Cansi Formation volcanics in the lower part and the Pandan Formation sedimentary rocks on the upper part in the central Cebu, and overlapped by Carcar Limestone in the north (Aurelio and Peña, 2010). The Early Cretaceous Tuburan Limestone, Cansi Basalt and Late Cretaceous Pandan Formation were found to have intercalated, gradational or conformable relation to each other, making up the Mananga Group as designated by Balce (1970). The Group occurs mainly in the central highlands, either in fault contact or unconformable to the younger formations. The Cansi Formation volcanics are mainly composed of basaltic flows, andesite and agglomerate, overly or intercalate with the Tuburan Orbitolina-rich limestone, roughly blanket the basement rocks in the central highlands. Petrographically, these volcanics are generally gray and fine-grained with occasionally porphyritic and amygdaloidal textures, ranging from typical basalt to pyroxene andesite. Thin layers of chert were also observed intercalating with the basalt. Observed alterations are silicification, pyritization, sericitization, kaolinization and chloritization with minor degree of epidotization (Aurelio and Peña, 2002). The Cansi Formation volcanics are unconformably overlain by the sedimentary units of the Pandan Formation, which are generally composed of limestone, shale and conglomerate, with occasional basalt and coal intercalations. Serpentinized peridotites broadly occur in the major fault zones of central Cebu, intruding the Tunlob Schist and Pandan Formation, in fault contact with the Cansi Formation volcanics and Tuburan limestone.

As reported from previous geological investigations, there are two intrusion phases in the Cebu Island, the Lutopan Diorite and Talamban Diorite, which occurred at an interval of ca. 93 Ma with lithologies varying from granodiorite to monzodiorite (Kerntke, 1992). The Lutopan Diorite is exposed in the Lutopan, Barot-Udlom, Sibakan and Kuanos-Mangilamon areas, and it is the ore-hosting rock of the porphyry Cu-Au deposit in the Atlas-Mining District with lithologies ranging from hornblende diorite to quartz diorite, intruding into the early stage Mananga Group volcanic and sedimentary rocks. Gervasio (1971) reported a K-Ar age of 59.5 Ma for the Lutopan Diorite. However, later radiometric K-Ar and Rb-Sr dating of three samples from Biga and Frank deposits in Atlas Mining District by Walther et al. (1981) indicated an age of 101–108 Ma, which is close to the zircon U-Pb age of 109 ± 2 Ma as reported by Kerntke (1992). Multiple intrusive phases are therefore suggested for the diorite bodies in Lutopan area (Aurelio and Peña, 2002). The Talamban Diorite is located only a few kilometers outside the Atlas-district, occurring as small stocks with lithologies ranging from diorite to quartz monzonite. Radiometric K-Ar dating (10.2–12.5 Ma, MMAJ-JICA, 1990) and Rb-Sr dating (13.1–13.7 Ma, Kerntke, 1992) of this rock indicated a late Middle Miocene age.

As reported by Deng et al. (2015), there were also small diorite outcrops in the Kansi area (Fig. 2), central northern part of the Cebu Island, which is about 12 km to the south of Tuburan, and about 40 km away to the northeast of the Atlas mining district. These diorites in Kansi intrude into the Mananga Group volcanics, especially the Cansi Formation volcanics (Figs. 2 and 3a), analogous to the geological condition of the Atlas porphyry Cu-Au deposit where the ore-bearing Lutopan Diorites also intrude into the Cansi Formation volcanics (Aurelio and Peña, 2002; Kerntke, 1992; Walther et al., 1981). The volcanic rocks in the Kansi area are widely altered by hydrothermal fluids (Deng et al., 2015), including mainly argillic, chloritic, albitic, siliceous and occasionally potassic alteration. Sulfide minerals associated with these alterations in the volcanic rocks occur as veins or disseminated pyrite, chalcopyrite and bornite. The copper mineralization can also be observed in the Kansi diorite porphyry, mainly in the form of malachite (Fig. 3b) due to supergene oxidation. Mineralized quartz veins have also been discovered in the area, with copper-bearing sulfides partly oxidized to malachite. Under the microscope, the Kansi diorite exhibits porphyritic texture with plagioclase and amphibole as phenocrysts. The amphibole phenocrysts are mostly altered to epidotes and opaque minerals, with amphibole pseudomorphs preserved (Fig. 4a and b). Most of the plagioclases are classified as albites from EPMA results (Table S1), suggesting albitization also occurred. The groundmass is composed of fine-grained plagioclase, amphibole, minor quartz, glass and opaque. The accessory minerals are apatite, magnetite and zircon.

3. Analytical methods

3.1. Major and trace elements

Whole rock major and trace elements were analyzed at the ALS Mineral Laboratory in Guangzhou. Fresh samples were powdered using an agate mill to grain sizes to <200 mesh. Major elements were determined using XRF spectrometry with standard deviations within 5%. The detailed methodology is as follows: Loss of ignition (LOI) was determined after igniting sample powders at 1000 °C for one hour. A calcined or ignited sample (0.9 g) was added to 9.0 g of Lithium Borate Flux ($Li_2B_4O_7$-$LiBO_2$), mixed well and fused in an auto fluxer between 1050–1100 °C. A flat molten glass disc was prepared from the resulting melt. This disc was then analyzed by wavelength-dispersive X-ray fluorescence spectrometry (XRF) using an AXIOS Minerals spectrometer. Trace elements, including REE, were determined by inductively coupled plasma mass spectrometry (ICP-MS) of solutions on an Elan DRC-II instrument (Element, Finnigan MAT) after 2-day closed beaker digestion using a mixture of HF and HNO_3 acids in Teflon screw-cap bombs. Detection limits, defined as 3 s of the procedural blank, for some critical elements are as follows (ppm): Th (0.05), Nb (0.2), Hf (0.2), Zr (2), La (0.5) and Ce (0.5). Accuracy and precision of the data are better than 5% for major elements and 10% for trace elements on the basis of analytical results and replicate analyses of international standard reference material (SRM) (Liu et al., 1996).

3.2. Zircon U-Pb isotopes

Zircon grains were separated from the sample KS123, mounted in epoxy resin, polished down to near half sections, and then photographed in reflected and transmitted light. The internal structure of zircon grains was examined using the cathodoluminescence (CL) image technique at the CAS Key Laboratory of Crust-Mantle Materials and Environments, University of Science and Technology of China (USTC). *In-situ* U-Pb dating and trace element analyses of zircons were conducted synchronously using an Agilent 7700 ICP-MS instrument equipped with a Geolas 2005 193 nm ArF-excimer laser (LA-ICP-MS) at the CAS Key Laboratory of Crust-Mantle Mate-

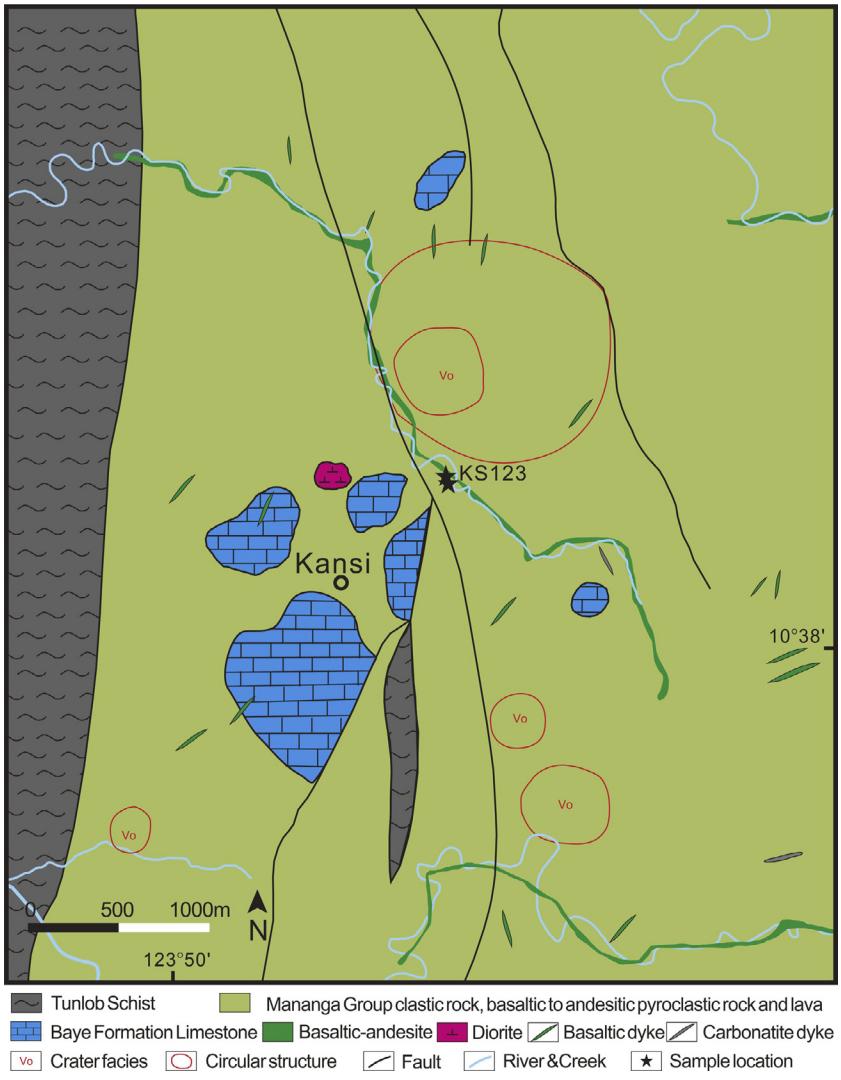

Fig. 2. Simplified geological map of the Kansi area. Modified after Deng et al. (2015).

rials and Environments, USTC. Detailed operating conditions for the laser ablation system and the ICP-MS instrument and data reduction were outlined by Gu et al. (2013). Sample mounts were placed in a special sample cell and flushed with Ar and He. Laser ablation was accomplished at a constant energy of 70 mJ, with a repetition rate of 10 Hz and a spot diameter of 32 μm. The ablated aerosol was carried to ICP-MS by He gas via a Squid system to smooth signals (Liang et al., 2009). Data were acquired for 30 s with the laser off, and 40 s with the laser on, giving approximately 100 mass scans. During the analyses, the standard silicate glass NIST (610, 612 and 614) was used to optimize the system. 91500 zircons and NIST SRM 610 glass were used as external calibration standards for U-Pb dating and trace element analysis, respectively, and ^{29}Si are used as the internal standard. Off-line selection and integration of background and analytical signals, and time-drift correction and quantitative calibration for trace element analyses and U-Pb dating were performed by ICPMSDataCal (Lin et al., 2008, 2010, 2016). Concordia diagrams and weighted mean calculations were made using Isoplot/Ex_ver3 (Ludwig, 2003).

3.3. Zircon Lu-Hf isotopes

After zircon U-Pb isotope measurement, the *in-situ* analyses of Lu-Hf isotopes were conducted by laser ablation of the same zircon domains on the previously analyzed U-Pb dating spots. Analyses were carried out using a New Wave-193 nm ArF-excimer laser-ablation system linked to a Neptune Multi-Collector Inductively Coupled Plasma Mass Spectrometer (LA-MC-ICP-MS), in the laboratory of the Tianjin Institute of Geology and Mineral Resource, Chinese Academy of Geological Sciences. Instrumental parameters and data acquisition followed that described by Geng et al. (2011). The analyses were conducted with beam diameter of 50 μm, 8 Hz repetition rate with a laser power of ~15 J/cm^2. External calibration was made by measuring zircon standard GJ-1 with the unknowns during the analyses to evaluate the reliability of the analytical data, which yielded a weighted mean ^{176}Hf/^{177}Hf ratio of 0.282001 ± 37 (2σ). This value is in good agreement with the recommended value of 0.282008 ± 7 (2σ, Wu et al., 2006). The corrections to raw Lu-Hf isotopic data followed the protocols of Geng et al. (2011) and Yuan et al. (2008). Isobaric interference of ^{176}Lu on ^{176}Hf was corrected by measuring the intensity of the interference-free ^{175}Lu isotope and using a recommended ^{176}Lu/^{175}Lu ratio of 0.02655 (Machado and Simonetti, 2001) to calculate ^{176}Lu/^{177}Hf ratios. The mean β_{Yb} value was applied for the isobaric interference correction of ^{176}Yb on ^{176}Hf in the same spot. The ratio of ^{176}Yb/^{172}Yb (0.5887) was also applied for the Yb correction. In calculation of $\varepsilon_{Hf}(t)$, the used decay constant value of ^{176}Lu is 1.867×10^{-11} yr^{-1} (Söderlund et al., 2004), the ^{176}Lu/^{177}Hf and

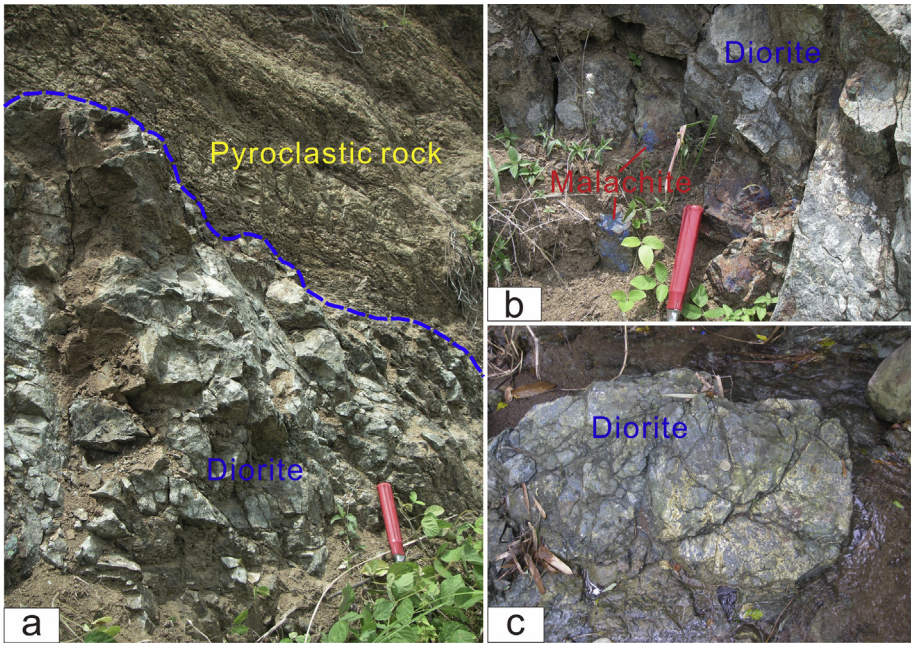

Fig. 3. Field photographs of the Kansi diorites, Cebu Island. a. Early stage Cansi Formation pyroclastic rock is intruded by the Kansi diorite. b. Altered diorite with malachite mineralization. c. Massive diorite in the bottom of a creek.

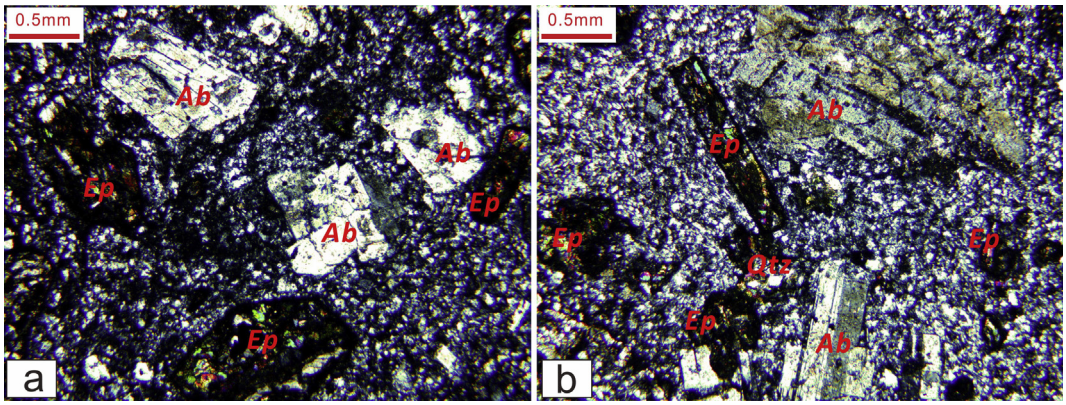

Fig. 4. Microphotographs of the Kansi diorites, Cebu Island. Mineral abbreviations: Ab – albite, Ep – epidote, Qtz – quartz.

$^{176}Hf/^{177}Hf$ values of chondrite are 0.0336 and 0.282785, respectively (Bouvier et al., 2008). Single-stage Hf model ages (TDM1) were calculated relative to the depleted mantle present-day value of $^{176}Hf/^{177}Hf = 0.28325$ (Nowell et al., 1998) and $^{176}Lu/^{177}Hf = 0.0384$ (Griffin et al., 2000).

3.4. Sr-Nd-Pb isotopes

All Sr-Nd-Pb isotopes were separated at the State Key Laboratory of Isotope Geochemistry, Guangzhou Institute of Geochemistry, Chinese Academy of Sciences (GIG-CAS). For Sr–Nd isotope determination, sample powders were initially dissolved in Teflon capsules with $HF + HNO_3$ acid. Following sample decomposition, strontium and REE were separated using cation columns, and then the Nd fractions were further separated using HDEHP-coated Kef columns. Lead was separated and purified by a conventional cation-exchange technique (AG18, 200–400 resin) with diluted HBr and HCl used as the eluants. Sr-Nd-Pb isotopic measurement was performed on a Thermo-Fisher Scientific Neptune Plus Multi-Collector Inductively-Coupled Plasma Mass Spectrometry (MC-ICP-MS) at the CAS Key Laboratory of Crust-Mantle Materials and Environments, USTC, following analytical procedures described by Wei et al. (2002), Liang et al. (2003) and He et al. (2005). Measured $^{87}Sr/^{86}Sr$ and $^{143}Nd/^{144}Nd$ ratios were normalized to $^{86}Sr/^{88}Sr = 0.1194$ and $^{146}Nd/^{144}Nd = 0.7219$ for mass fractionation, respectively. The reported $^{87}Sr/^{86}Sr$ and $^{143}Nd/^{144}Nd$ ratios were respectively adjusted to the NBS SRM 987 standard with an $^{87}Sr/^{86}Sr$ value of 0.710248 and the Shin Etsu JNdi-1 standard with a $^{143}Nd/^{144}Nd$ value of 0.512115. The mean values of the Sr and Nd standards NBS 987 and JNdi-1 during period of analysis are $^{87}Sr/^{86}Sr = 0.710245 \pm 10$ (n = 12) and $^{143}Nd/^{144}Nd = 0.512115 \pm 2$ (n = 21), respectively. The $^{87}Rb/^{86}Sr$ and $^{147}Sm/^{144}Nd$ ratios were calculated using the whole-rock Rb, Sr, Sm and Nd concentrations obtained by ICP-MS. During Pb isotopes analysis, the reported $^{206}Pb/^{204}Pb$, $^{207}Pb/^{204}Pb$, $^{208}Pb/^{204}Pb$ were adjusted to the NBS SRM 981 standard with $^{206}Pb/^{204}Pb$, $^{207}Pb/^{204}Pb$ and $^{208}Pb/^{204}Pb$ values of 16.9405, 15.4963 and 36.7219, respectively. Precision of the measured Pb isotopic ratios was better than 0.01%.

4. Results

4.1. Major and trace elements

Five diorite porphyry samples from the Kansi area were analyzed for major and trace element compositions, and the results are listed in Table 1. The diorite porphyries have SiO_2 contents ranging from 56.7 to 58.9 wt% (av. 57.8 wt%), showing intermediate-felsic compositions. They all have high Al_2O_3 contents (16.1–16.3 wt%), high MgO contents (3.36–3.86 wt%) and Mg# (56.2–60.2), which are similar to the compositions of high-Mg andesites (Kelemen, 1995; Tatsumi, 2006). The Kansi diorites are sodium rich with Na_2O contents ranging from 3.61–5.68 wt% (av. 4.79 wt%), and their K_2O contents (0.25–0.58 wt%) are relatively low, probably lost due to alteration during post-magmatic mineralization stage. In addition, the negative anomalies of mobile elements like Rb and Ba observed in Fig. 7b are also probably caused by alteration, similar to the condition of low K_2O contents. In view of the fact that K as well as other mobile elements such as Na, Rb, Ba and Sr have been unpredictably added and/or extracted during hydrothermal alteration, the TAS, K_2O-SiO_2 diagrams for rock classification are not useful (Hastie et al., 2007). Therefore, discrimination diagrams of more immobile elements for the altered or weathered igneous rocks are used in this paper. As shown in Fig. 5a, the Kansi diorite porphyries are all calc-alkaline series, with chemical compositions equivalent to "andesite" (Fig. 5b). The Lutopan diorites in the Atlas mining district are diorites to quartz-diorites in composition, equivalent to "andesite" to "rhyodacite" as shown in Fig. 5b. Besides, their Fe_2O_3, CaO, TiO_2, MnO and P_2O_5 contents range from 5.02 to 5.57 wt%, 4.53 to 5.73 wt%, 0.46 to 0.54 wt%, 0.09 to 0.10 wt% and 0.22 to 0.23 wt%, respectively. The continuous variations of major elements of Kansi and Lutopan diorites on the Harker diagram roughly define the same trend (Fig. 6), suggesting that these two diorites were probably generated from a uniform source but experienced different degrees of partial melting or fractional crystallization .

The Kansi diorites show high LREE contents and low HREE contents with $(La/Yb)_N$ ratios ranging from 9.7 to 12.8, displaying LREE enrichment and HREE depletion on Fig. 7a, with no negative Eu anomalies observed. They have positive anomalies of Pb, Sr, Zr and Hf and negative anomalies of Nb, Ta and Ti on Fig. 7b, which are typical features of arc-related rocks. The Kansi diorites, together with the Lutopan diorites, are classified as adakites for the high Sr/Y and $(La/Yb)_N$ ratios, and low Y and Yb contents (Fig. 8a and b). Given the moderate to high SiO_2 contents and high to moderate MgO contents, the Kansi and Lutopan diorites are identified as high silica adakites (HSA, Fig. 9a) (Defant and Drummond, 1990; Martin et al., 2005; Moyen, 2009). Their Mg# are systematically higher than those of experimental oceanic crust melts at 1–4 GPa, and projected in the field defined by modern island arc adakites (Fig. 9b).

Table 1
Major and trace element contents of the Kansi diorites, Cebu island.

Sample No.		KS123-1	KS123-3	KS123-4	KS123-05	KS123-06
Major						
SiO_2	%	57.3	58.3	57.8	58.9	56.7
Al_2O_3	%	16.4	16.6	16.1	16.1	16.2
Fe_2O_3	%	5.57	5.30	5.02	5.02	5.36
CaO	%	4.73	5.73	5.27	4.95	4.53
MgO	%	3.60	3.78	3.36	3.82	3.86
Na_2O	%	5.58	3.61	5.68	3.91	5.49
K2O	%	0.41	0.58	0.25	0.56	0.43
TiO_2	%	0.47	0.51	0.46	0.52	0.54
MnO	%	0.10	0.10	0.10	0.09	0.10
P_2O_5	%	0.22	0.22	0.22	0.23	0.22
LOI	%	4.85	4.85	4.57	4.89	5.76
Total	%	99.2	99.6	98.8	99.0	99.1
Mg#		56.2	58.6	57.1	60.2	58.8
Trace						
V	ppm	103	111	101	114	126
Cr	ppm	56	62	52	80	80
Ni	ppm	34.2	38.1	33.4	50.0	48.0
Co	ppm	14.8	15.1	13.7	13.1	12.9
Cs	ppm	0.05	0.05	0.05	0.03	0.02
Rb	ppm	3.0	4.9	1.4	7.8	5.3
Ba	ppm	120	50	40	54	103
Th	ppm	0.80	1.20	0.80	2.06	2.01
U	ppm	0.40	0.40	0.40	0.66	0.67
Nb	ppm	1.8	1.9	1.8	1.9	1.9
Ta	ppm	0.14	0.15	0.14	0.15	0.14
La	ppm	14.4	15.1	14.1	18.3	17.5
Ce	ppm	33.1	37.0	34.5	44.9	42.7
Pb	ppm	3.5	2.1	3.5	3.7	3.6
Pr	ppm	4.36	4.69	4.33	5.20	4.90
Nd	ppm	17.0	18.7	17.2	23.4	23.1
Sr	ppm	531	393	502	500	570
Sm	ppm	3.38	3.78	3.40	4.30	4.50
Hf	ppm	3.5	3.6	3.5	3.9	4.5
Zr	ppm	150.1	147.2	145.3	159.0	175.0
Eu	ppm	0.96	1.05	0.99	1.10	1.10
Gd	ppm	2.58	2.93	2.67	3.20	3.50
Tb	ppm	0.36	0.39	0.35	0.40	0.40
Dy	ppm	1.98	2.14	1.95	2.40	2.50
Ho	ppm	0.36	0.41	0.36	0.40	0.50
Y	ppm	9.3	10.9	9.3	12.8	13.3
Er	ppm	0.94	1.10	0.95	1.30	1.40
Tm	ppm	0.13	0.15	0.13	0.20	0.20
Yb	ppm	0.82	0.93	0.79	1.20	1.30
Lu	ppm	0.11	0.13	0.12	0.20	0.20

4.2. Zircon U-Pb geochronology and trace elements

Zircon grains separated from the diorite porphyry sample KS123-1 are mostly prismatic, colorless, transparent, and euhedral to sub-euhedral. Results of zircon LA-ICP-MS U-Pb isotope data are listed in Table 2. From the Cathodoluminescence (CL) images and zircon age results, three types of zircons have been distinguished: (1) Magmatic zircons with no relict core, which clearly show microscale oscillatory zonations and yield single spot $^{206}Pb/^{238}U$ ages of 106–114 Ma (Fig. 10a). Analyses of 12 spots yielded a zircon U-Pb concordant age of 109.5 ± 1.9 Ma, with a weighted mean $^{206}Pb/^{238}U$ ages of 110.3 ± 4.1 Ma (Fig. 10c), indicating an emplacement age of the Early Cretaceous for the diorite porphyry. (2) Magmatic zircons with a dark colored xenocrystic core and a narrow light colored magmatic rim (second line in Fig. 10b). These cores are mostly rounded in shape, showing broad or vague oscillatory zonations, with single spot $^{206}Pb/^{238}U$ ages of 116–125 Ma (second line in Fig. 10b). (3) Single xenocrystic zircons with simple magmatic textures, yield single spot $^{206}Pb/^{238}U$ ages of 113–126 Ma (first line in Fig. 10b). Apart from one rounded large zircon, most of them are elongated grains, showing broad oscillatory zonations from the CL images (first line in Fig. 10b), which also indicate magmatic origins. All these xenocrystic cores and zircons yield concordant U-Pb ages, showing unimodal distribution of $^{206}Pb/^{238}U$ ages with a peak at ca.118 Ma (Fig. 10d), consistent with the formation age of Kansi volcanics in the area (Deng et al., 2015), which are the wallrocks of the diorite porphyry.

Zircon trace elements results analyzed simultaneously with zircon U-Pb isotopes are listed in Table 3. All the zircons from the diorite sample KS123-1 show LREE depletion and HREE enrichment on the chondrite-normalized REE distribution pattern (Fig. 16a), with pronounced positive anomaly of Ce and slight negative anomaly of Eu, typical of magmatic zircons. The magmatic zircons formed during diorite crystallization have systematically low LREE (La, Pr and Nd, except Ce) contents than those of the xenocrystic zircons, while their MREE (Sm, Eu, Gd, Tb, Dy) and HREE (Ho, Er,

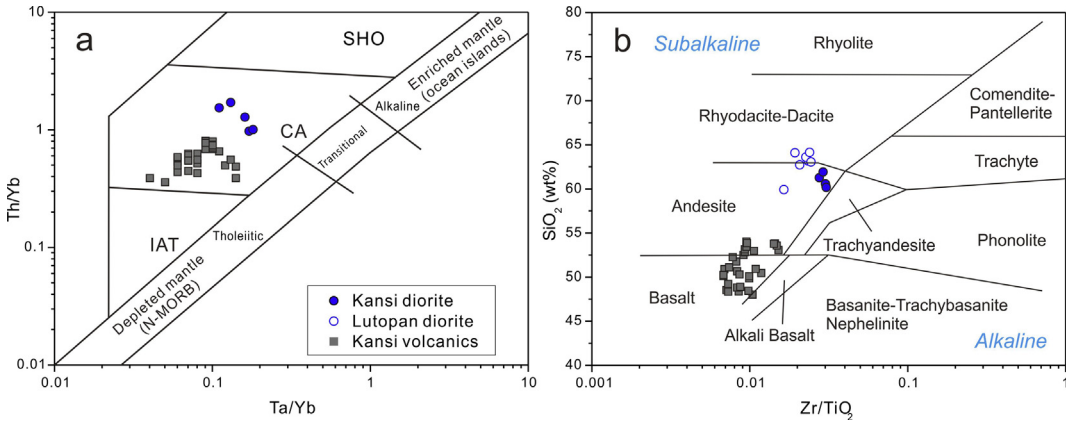

Fig. 5. Classification diagrams of the Kansi diorites, Cebu Island. a. Th/Yb-Ta/Yb diagram, after Pearce (1982). IAT – Island arc tholeiite, CA – Calc-alkaline series, SHO – Shoshonitic series. b. SiO_2-Zr/TiO_2 diagram, after Winchester and Floyd (1977). Data of the Kansi volcanics are from Deng et al. (2015), and data of the Lutopan diorites are from Walther et al. (1981) and Kerntke et al. (1991), as are other major and trace elements below.

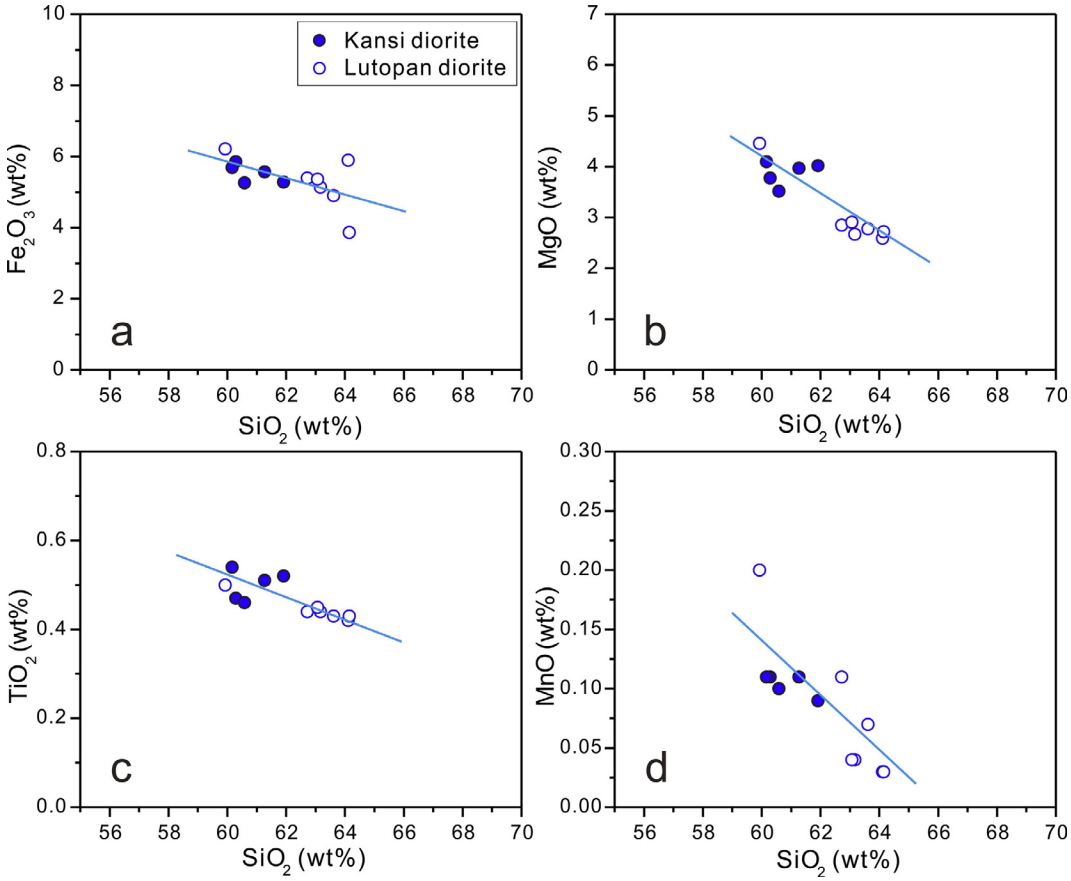

Fig. 6. Major element Harker diagrams of the Kansi diorites, Cebu Island.

Tm, Yb, Lu) contents are mostly in the same ranges, respectively, as observed from Table 3 and Fig. 16a.

4.3. Zircon Lu-Hf isotopes

Zircon Lu-Hf isotopic results of sample KS123-1 are listed in Table 4. The $\varepsilon_{Hf}(t)$ (t = 110 Ma) values of the magmatic zircons formed during magma crystallization are close to the area of Amami plateau tonalite (Fig. 11a), ranging from + 9.8 to + 15.2 (mean + 12.4), with T_{DMI} ages from 394 Ma to 160 Ma, signifying a highly depleted magma source dominated by juvenile components. The $\varepsilon_{Hf}(t)$ values of the xenocrystic cores and zircons are systematically lower than those of the magmatic zircons (Fig. 11a and b), ranging from +6.1 to +12.8 (mean + 9.5), with higher T_{DMI} ages (Fig. 11c) from 550 Ma to 272 Ma (Table 4). The $\varepsilon_{Hf}(t)$ values of these xenocrystic zircons are in the range of Kansi volcanics and river sands as reported by our former work (Deng et al., 2015).

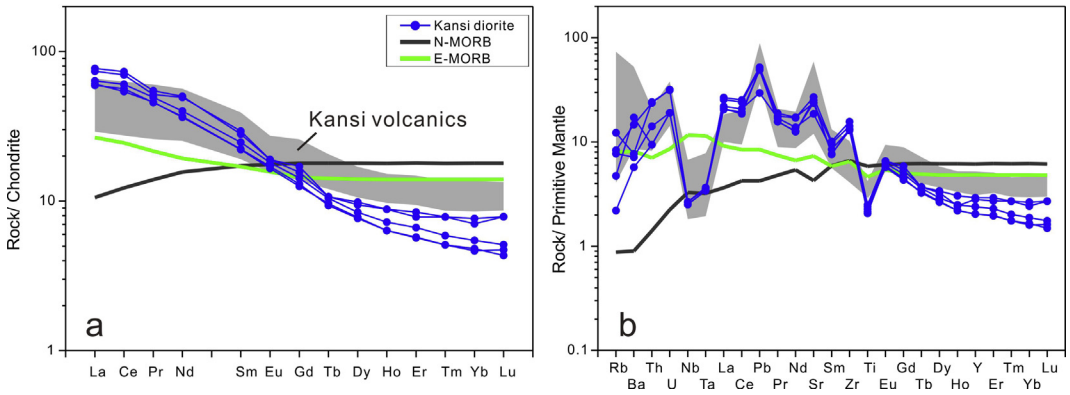

Fig. 7. Chondrite normalized REEs (a) and primitive mantle normalized trace elements (b) distribution patterns of the Kansi diorites, Cebu Island. Chondrite and primitive mantle-normalized data are taken from Sun and McDonough (1989).

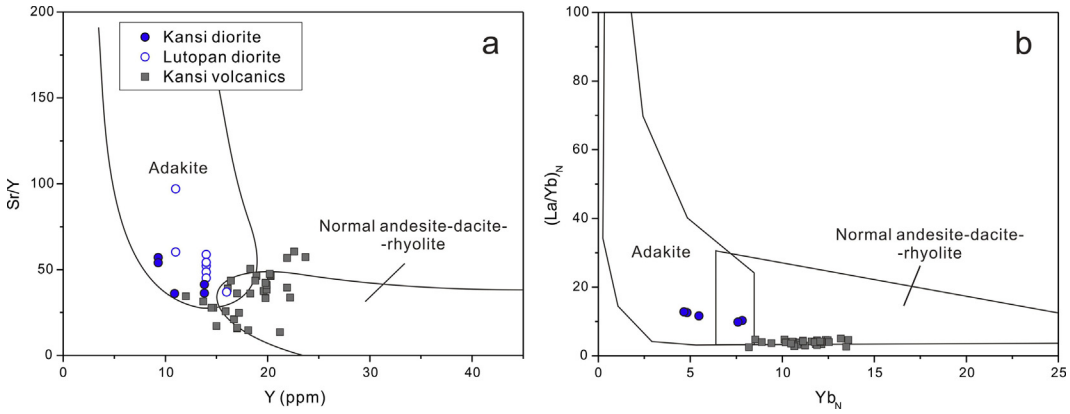

Fig. 8. Sr/Y-Y (a) and $(La/Yb)_N$-Yb_N (b) classification diagrams for the Kansi diorites, after Defant and Drummond (1990).

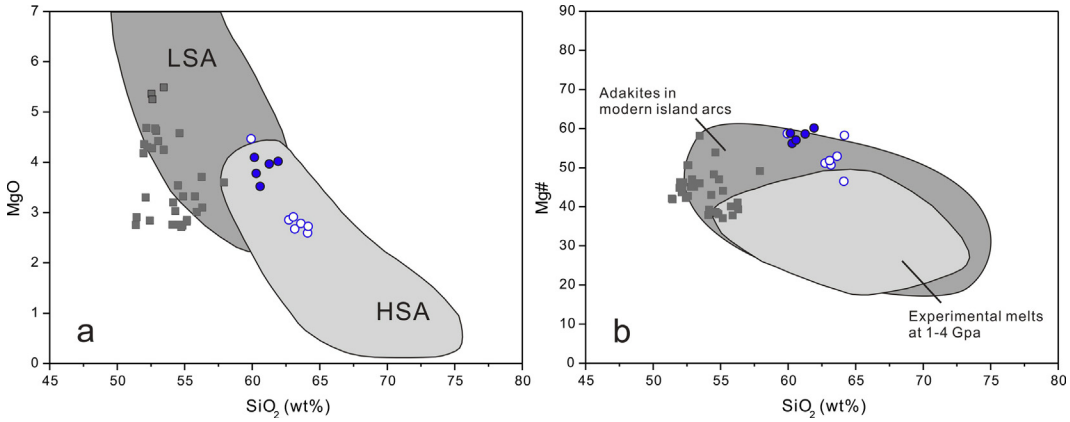

Fig. 9. MgO (wt%) and Mg# versus SiO_2 (wt%) diagrams for the Kansi diorites. LSA- low silica adakite, HSA- high silica adakite. The fields of LSA and HSA are from Martin et al. (2005). The field of modern island arc adakites is after Defant and Kepezhinskas (2001). The area of experimental OC (represented by metabasalt with MORB compositions) melts (1–4 GPa) is from Rapp et al. (1999).

4.4. Sr-Nd-Pb isotopes

Whole rock Sr-Nd-Pb isotopic data of the Kansi diorites are shown in Table 5. The $(^{87}Sr/^{86}Sr)_i$ and $\varepsilon_{Nd}(t)$ values of the Kansi diorites vary in a narrow range from 0.70315 to 0.70316 and +7.2 to +7.5, respectively. They are plotted in the area between Pacific MORB and Indian MORB, closed to the area of Amami Plateau basalt and tonalite (Fig. 12). The Kansi diorites have variable Pb isotope compositions with $(^{206}Pb/^{204}Pb)_i$ = 18.320–18.550, $(^{207}Pb/^{204}Pb)_i$ = 18.509–18.571 and $(^{208}Pb/^{204}Pb)_i$ = 37.986–38.228, which are also plotted between the area of Pacific MORB and Indian MORB.

5. Discussion

5.1. Kansi diorites: typical high-Mg adakites

Adakites are characterized by >56% SiO_2, ≥15% Al_2O_3 (rarely lower), usually <3% MgO (rarely above 6% MgO), low Y and HREE

Table 2
Zircon LA-ICP-MS U-Pb isotopic compositions of the Kansi diorite, Cebu Island.

Spot NO.	^{232}Th	^{238}U	^{232}Th/^{238}U Ratio	^{207}Pb/^{235}U Ratio	^{207}Pb/^{235}U 1σ	^{206}Pb/^{238}U Ratio	^{206}Pb/^{238}U 1σ	^{207}Pb/^{235}U Age (Ma)	^{207}Pb/^{235}U 1σ	^{206}Pb/^{238}U Age (Ma)	^{206}Pb/^{238}U 1σ
Magmatic zircon											
KS123-01	57.8	70.6	0.8	0.12735	0.02365	0.01665	0.00105	122	21	106	7
KS123-02	51.6	78.6	0.7	0.12072	0.02796	0.01738	0.00136	116	25	111	9
KS123-04	25.9	45.6	0.6	0.11705	0.02377	0.01736	0.00102	112	22	111	6
KS123-05	44.8	63.7	0.7	0.11730	0.03401	0.01698	0.00128	113	31	109	8
KS123-06	168.8	131.5	1.3	0.12312	0.01497	0.01755	0.00087	118	14	112	6
KS123-07	17.1	36.9	0.5	0.11727	0.04897	0.01686	0.00098	113	45	108	6
KS123-08	12.0	28.6	0.4	0.12028	0.02877	0.01728	0.00149	115	26	110	9
KS123-10	35.6	58.5	0.6	0.11355	0.02737	0.01729	0.00148	109	25	111	9
KS123-14	234.4	268.7	0.9	0.11282	0.01066	0.01762	0.00080	109	10	113	5
KS123-23	17.3	37.3	0.5	0.11638	0.02879	0.01747	0.00120	112	26	112	8
KS123-25	13.9	28.4	0.5	0.11581	0.05506	0.01707	0.00171	111	50	109	11
KS123-27	96.0	137.6	0.7	0.11335	0.03952	0.01667	0.00141	109	36	107	9
Xenocrystic zircon											
KS123-03	33.4	45.4	0.7	0.12407	0.02155	0.01809	0.00113	119	19	116	7
KS123-09	39.7	55.4	0.7	0.12765	0.02726	0.01961	0.00118	122	25	125	7
KS123-12	48.1	61.5	0.8	0.11047	0.02215	0.01812	0.00108	106	20	116	7
KS123-13	79.9	102.7	0.8	0.11986	0.02982	0.01771	0.00118	115	27	113	7
KS123-15	22.5	31.2	0.7	0.14416	0.05541	0.01893	0.00202	137	49	121	13
KS123-16	33.4	55.0	0.6	0.12531	0.02964	0.01821	0.00123	120	27	116	8
KS123-17	54.0	57.9	0.9	0.13813	0.03063	0.01815	0.00104	131	27	116	7
KS123-18	44.6	63.7	0.7	0.12521	0.02285	0.01885	0.00107	120	21	120	7
KS123-19	50.7	80.0	0.6	0.12364	0.02704	0.01952	0.00126	118	24	125	8
KS123-20	30.3	45.0	0.7	0.12588	0.01738	0.01845	0.00094	120	16	118	6
KS123-24	87.8	92.5	0.9	0.13363	0.02736	0.01878	0.00130	127	25	120	8
KS123-26	74.1	89.0	0.8	0.13116	0.04111	0.01947	0.00156	125	37	124	10
KS123-29	107.5	133.7	0.8	0.12235	0.02281	0.01870	0.00125	117	21	119	8
KS123-32	117.1	109.9	1.1	0.13386	0.04578	0.01977	0.00125	128	41	126	8

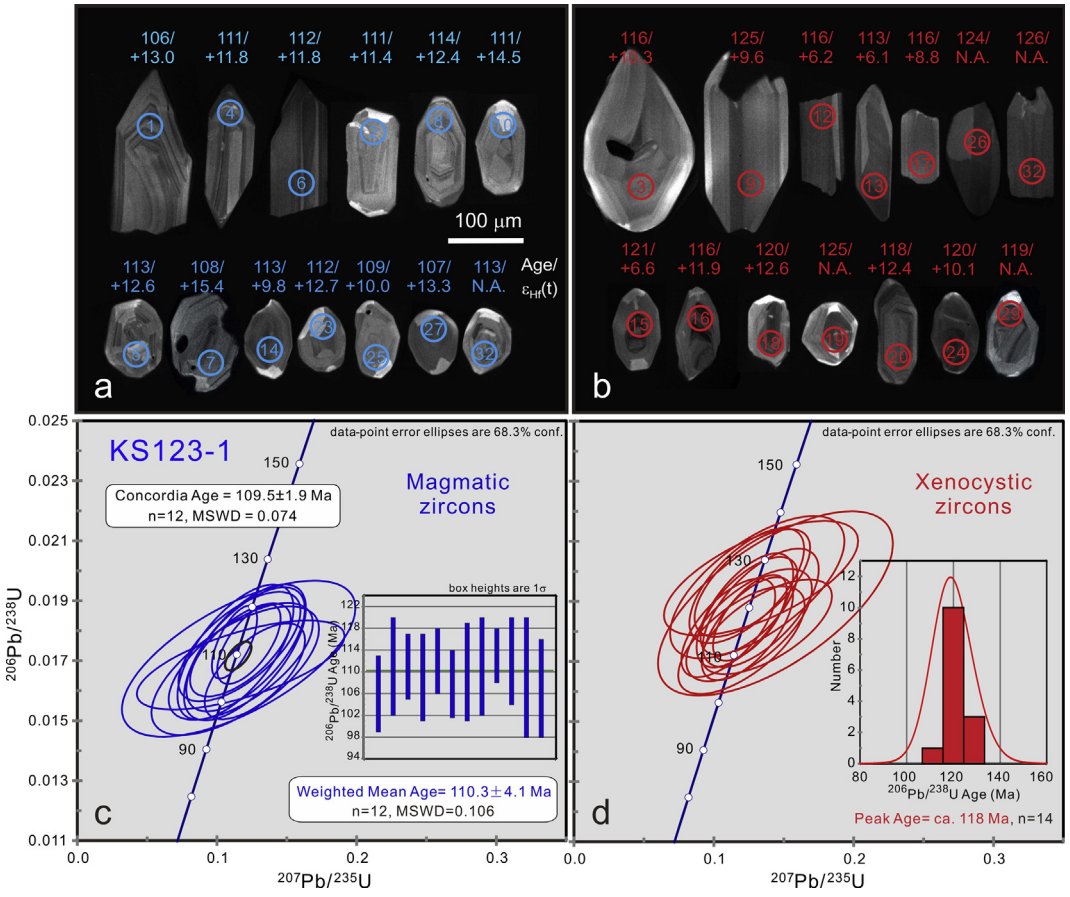

Fig. 10. Zircon CL images and LA-ICP-MS U-Pb concordia diagrams of the Kansi diorites.

Table 3
Zircon LA-ICP-MS trace element compositions of the Kansi diorite, Cebu Island.

Spot NO.	P ppm	Ti ppm	Nb ppm	Ta ppm	La ppm	Ce ppm	Pr ppm	Nd ppm	Sm ppm	Eu ppm	Gd ppm	Tb ppm	Dy ppm	Ho ppm
Magmatic zircon														
KS123-01	532	12.2	0.56	0.07	0.089	15.5	0.13	2.2	4.8	2.4	28.6	9.0	101.8	37.4
KS123-02	555	12.1	0.66	0.11	0.014	13.7	0.12	1.9	3.4	2.0	22.4	6.8	87.3	34.4
KS123-04	297	12.0	0.28	0.07	0.012	9.3	0.07	1.6	2.1	1.3	14.5	4.9	55.9	21.2
KS123-05	505	10.0	0.53	0.11	0.006	14.0	0.10	1.8	4.5	2.1	23.5	7.3	86.9	32.6
KS123-06	800	11.2	0.62	0.16	0.086	41.5	0.95	15.4	26.6	10.9	89.7	23.8	237.9	78.6
KS123-07	318	10.0	0.33	0.08	0.006	6.2	0.08	1.3	2.6	1.2	11.3	3.5	42.3	16.5
KS123-08	357	10.8	0.40	0.09	0.013	5.5	0.03	1.0	1.9	0.9	8.1	2.4	30.2	13.1
KS123-10	345	8.5	0.34	0.12	0.024	9.2	0.07	1.4	3.3	1.5	14.8	4.8	55.1	21.2
KS123-14	677	10.1	1.38	0.38	0.020	39.2	0.16	3.0	10.8	5.3	58.1	16.4	181.9	65.2
KS123-23	358	9.8	0.29	0.08	0.009	6.0	0.09	1.3	2.6	1.2	11.8	3.6	43.6	16.7
KS123-25	205	8.9	0.52	0.01	0.013	4.7	0.06	0.9	1.5	0.9	6.0	2.3	23.9	9.6
KS123-27	381	8.6	0.91	0.24	0.012	20.7	0.10	2.0	6.3	2.5	30.8	9.7	113.4	42.2
Av.	**444**	**10.4**	**0.57**	**0.13**	**0.025**	**15.5**	**0.16**	**2.8**	**5.9**	**2.7**	**26.7**	**7.9**	**88.4**	**32.4**
Xenocrystic zircon														
KS123-03	279	10.8	0.31	0.14	0.032	9.5	0.33	4.6	5.2	3.1	25.5	7.5	80.6	29.2
KS123-09	436	9.7	0.31	0.06	0.002	12.2	0.39	5.4	7.6	3.6	28.5	8.2	86.1	29.2
KS123-12	381	8.9	0.52	0.10	0.038	14.0	0.35	6.6	9.7	3.8	31.0	9.1	93.4	32.2
KS123-13	503	10.0	0.68	0.12	0.049	18.7	0.48	7.8	10.9	5.3	44.4	12.4	129.6	46.5
KS123-15	183	7.4	0.20	0.05	0.020	4.5	0.05	0.7	1.0	0.5	5.2	1.6	18.2	7.5
KS123-16	460	12.3	0.43	0.06	0.015	10.3	0.14	2.1	3.6	1.8	16.1	5.4	64.9	26.0
KS123-17	316	9.6	0.35	0.07	0.038	13.8	0.39	6.1	10.5	4.3	32.7	8.5	92.7	32.7
KS123-18	374	8.8	0.39	0.12	0.019	12.9	0.24	3.9	5.6	2.7	21.1	7.0	72.7	27.2
KS123-19	396	11.2	0.50	0.11	0.326	12.9	0.14	2.1	4.2	1.6	18.3	5.1	55.2	21.8
KS123-20	344	9.5	0.29	0.09	0.035	8.7	0.15	2.5	4.0	1.9	16.1	4.9	52.7	20.4
KS123-24	445	8.8	0.56	0.11	0.092	18.9	0.55	9.3	12.7	6.2	42.8	10.5	102.1	34.8
KS123-26	358	13.4	0.62	0.15	0.068	21.8	0.60	10.5	14.0	6.6	50.0	13.7	147.1	50.5
KS123-29	408	6.9	0.74	0.17	0.004	22.4	0.13	2.5	6.3	2.6	31.3	10.1	115.0	42.8
KS123-32	588	6.3	0.76	0.11	0.128	22.6	0.71	11.6	17.5	8.3	53.5	13.7	127.0	42.3
Av.	**390.8**	**9.5**	**0.5**	**0.1**	**0.1**	**14.5**	**0.3**	**5.4**	**8.1**	**3.7**	**29.8**	**8.4**	**88.4**	**31.6**

Spot NO.	Er ppm	Tm ppm	Yb ppm	Lu ppm	Hf ppm	Th ppm	U ppm	Th/U	$T_{Ti\ in\ Zircon}$ °C	δCe	δEu	lg(fO_2)	ΔFMQ
Magmatic zircon													
KS123-01	169.4	36.4	387.9	77.5	10980	58	71	0.8	759	107	0.61	-9.9	5.5
KS123-02	172.7	38.5	434.8	90.4	7489	52	79	0.7	758	156	0.62	-8.5	6.9
KS123-04	105.8	24.5	289.8	61.6	9140	26	46	0.6	757	135	0.58	-9.1	6.3
KS123-05	156.0	33.8	375.8	77.4	11190	45	64	0.7	741	126	0.60	-10.2	5.7
KS123-06	337.3	70.5	760.5	144.9	10160	169	131	1.3	751	23	0.69	-16.1	-0.5
KS123-07	84.1	19.5	233.6	49.8	11236	17	37	0.5	741	87	0.59	-11.6	4.2
KS123-08	70.8	17.3	198.7	44.6	6793	12	29	0.4	748	125	0.64	-9.9	5.8
KS123-10	102.7	23.5	254.8	56.0	11103	36	59	0.6	727	109	0.61	-11.4	4.7
KS123-14	282.0	57.9	619.5	120.8	13649	234	269	0.9	742	149	0.76	-9.5	6.3
KS123-23	85.3	19.8	238.1	50.6	10636	17	37	0.5	739	85	0.61	-11.7	4.1
KS123-25	48.8	11.7	134.9	30.8	9373	14	28	0.5	731	105	0.75	-11.4	4.7
KS123-27	193.5	41.4	472.0	93.8	13500	96	138	0.7	728	149	0.59	-10.2	5.9
Av.	**150.7**	**32.9**	**366.7**	**74.8**	**10437**	**65**	**82**	0.8	**744**	**113**	**0.64**	**-10.8**	**5.0**
Xenocrystic zircon													
KS123-03	137.8	30.7	343.0	69.9	10109	33	45	0.7	748	31	0.67	-15.1	0.6
KS123-09	135.6	30.5	351.8	71.2	8071	40	55	0.7	738	28	0.69	-16.0	-0.1
KS123-12	145.8	31.5	359.8	72.4	10232	48	61	0.8	731	23	0.61	-17.1	-1.0
KS123-13	209.3	44.4	499.5	99.1	9939	80	103	0.8	741	28	0.66	-15.8	0.0
KS123-15	38.5	9.1	111.2	25.5	7630	23	31	0.7	715	147	0.52	-10.9	5.5
KS123-16	131.2	29.0	339.8	70.5	8355	33	55	0.6	759	93	0.60	-10.4	5.0
KS123-17	142.2	30.8	354.0	70.5	7026	54	58	0.9	737	23	0.69	-16.8	-0.9
KS123-18	129.1	27.8	330.1	68.4	9458	45	64	0.7	730	48	0.64	-14.4	1.7
KS123-19	104.4	23.6	273.4	57.7	11821	51	80	0.6	751	90	0.54	-10.9	4.6
KS123-20	94.5	21.9	249.3	52.6	8619	30	45	0.7	736	52	0.64	-13.8	2.2
KS123-24	147.6	31.7	347.0	73.2	7763	88	93	0.9	729	18	0.80	-18.1	-2.0
KS123-26	222.6	49.1	529.6	107.8	10136	74	89	0.8	767	23	0.69	-15.3	-0.1
KS123-29	194.4	42.1	440.2	91.4	10514	108	134	0.8	709	130	0.55	-11.7	4.9
KS123-32	180.7	37.1	420.4	85.5	6991	117	110	1.1	702	15	0.84	-20.1	-3.3
Av.	**143.8**	**31.4**	**353.5**	**72.6**	**9047.5**	**58.8**	**73.1**	**0.8**	**735.3**	**53.4**	**0.7**	**-14.7**	**1.2**

(for example, Y and Yb lower than 18 and 1.9 ppm, respectively) and high Sr (usually ≥ 400 ppm) than normal arc andesite-dacite-rhyolites (ADRs), low high-field strength elements (HFSEs) as in most island arc ADRs, and $^{87}Sr/^{87}Sr$ usually ≤ 0.7040. The Kansi diorites are characterized by moderate SiO_2 contents (56.7–58.9 wt%), high Al_2O_3 contents (16.1–16.6 wt%), low Y and Yb contents (9.3–13.3 ppm, 0.79–1.30 ppm, respectively), high Sr contents (393–570 ppm), high Sr/Y and La/Yb ratios (Fig. 8), low ($^{87}Sr/^{86}Sr)_i$ ratios (0.7032) with depletion of Nb, Ta, and Ti (Fig. 7b), typical of adakites from partial melting of garnet- or amphibole-bearing metabasalt, similar to other adakites from modern island arcs, e.g., Aleutians Islands (Kay, 1978); Papua New Guinea, Alaska and Woodlark Basin (Defant and Drummond, 1990); Kamchatka Arc (Drummond et al., 1996; Kepezhinskas et al., 1995); Andean

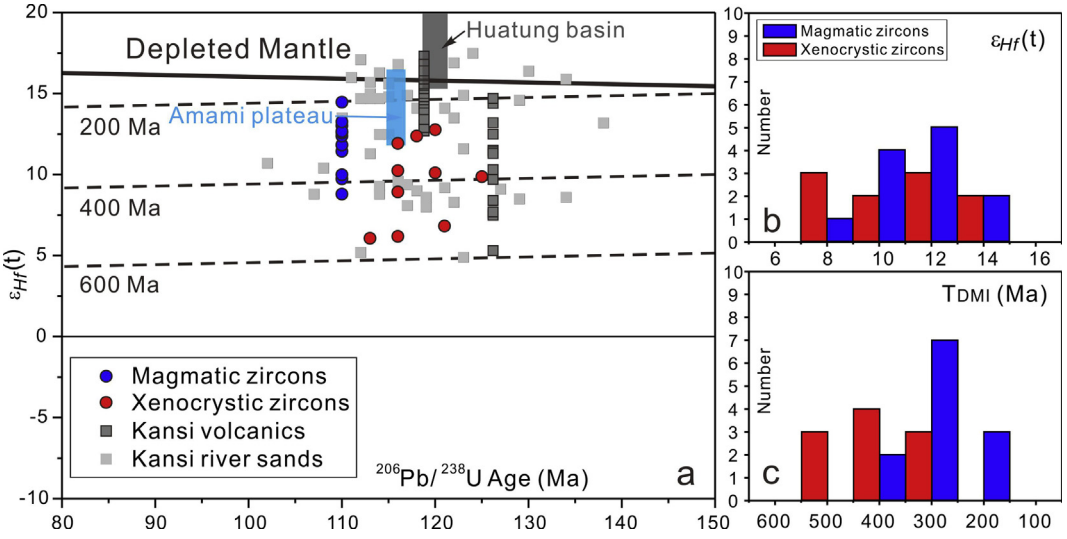

Fig. 11. Zircon Hf isotopic compositions (a) and histograms of $\varepsilon_{Hf}(t)$ and Hf model ages (T_{DMI}) (b, c) of the Kansi diorites. The areas of Amami Plateau and Huatung basin are from Hickey-Vargas et al. (2008), based on the ages and $\varepsilon_{Hf}(t)$ values of the Amami Plateau basalts and tonalites, Huatung basin gabbros, respectively, so are the Sr-Nd-Pb isotopes bellow. The data of Kansi volcanics and river sands are from Deng et al. (2015).

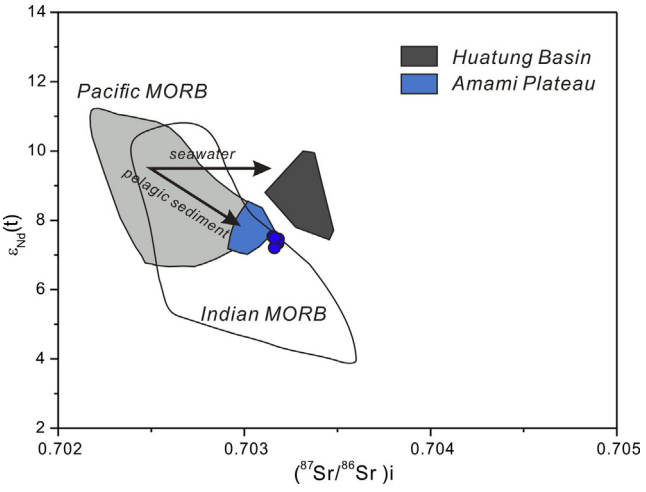

Fig. 12. Initial Sr-Nd isotopic compositions of the Kansi diorites, Cebu Island.

Austral Volcanic Zone, Chile (Drummond et al., 1996; Stern and Kilian, 1996); Pichincha, Ecuador (Bourdon et al., 2002); Baja California and Mezcala, Mexcico (Aguillon-Robles et al., 2001; Gonzalez-Partida et al., 2003); Northern and Southern Philippine arcs (Gregoire et al., 2008; Maury et al., 1996; Sajona et al., 1993, 2000b; Schiano et al., 1995), etc.

The high MgO contents (3.36–3.86 wt%) and Mg# (56.2–60.2 wt %) of Kansi adakites, with additional high Cr (52–80 ppm) and Ni (33–50 ppm) contents, are the characteristics of high-Mg adakites. The Mg#, MgO, Cr, and Ni contents of the Kansi adakites are clearly higher than in experimental melts from metabasalt (Rapp et al., 1999; Sen and Dunn, 1994), which probably reflect the interaction between pristine slab melts and mantle peridotite (Defant and Drummond, 1990; Defant and Kepezhinskas, 2001; Martin et al., 2005; Stern and Kilian, 1996). The Lutopan diorites in the Atlas mining district show similar adakitic features to the Kansi diorites (Fig. 8a), with higher SiO_2 contents and lower MgO contents and Mg# (Fig. 9a and b), suggesting a higher degree of fractional crystallization.

5.2. Petrogenesis of the Kansi diorites

For adakites generated in the island arc settings, three main petrogenesis have been presented: (1) partial melting of subducted oceanic crust in hot subduction zones (Defant and Drummond, 1990) or some other specific situations where the slab is abnormally heated, such as flat subduction at shallow depths

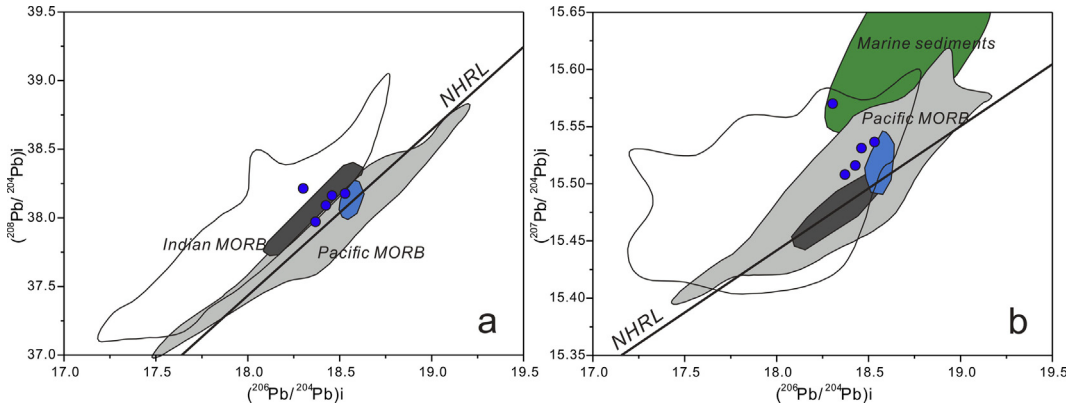

Fig. 13. Pb isotopic compositions of the Kansi diorites, Cebu Island.

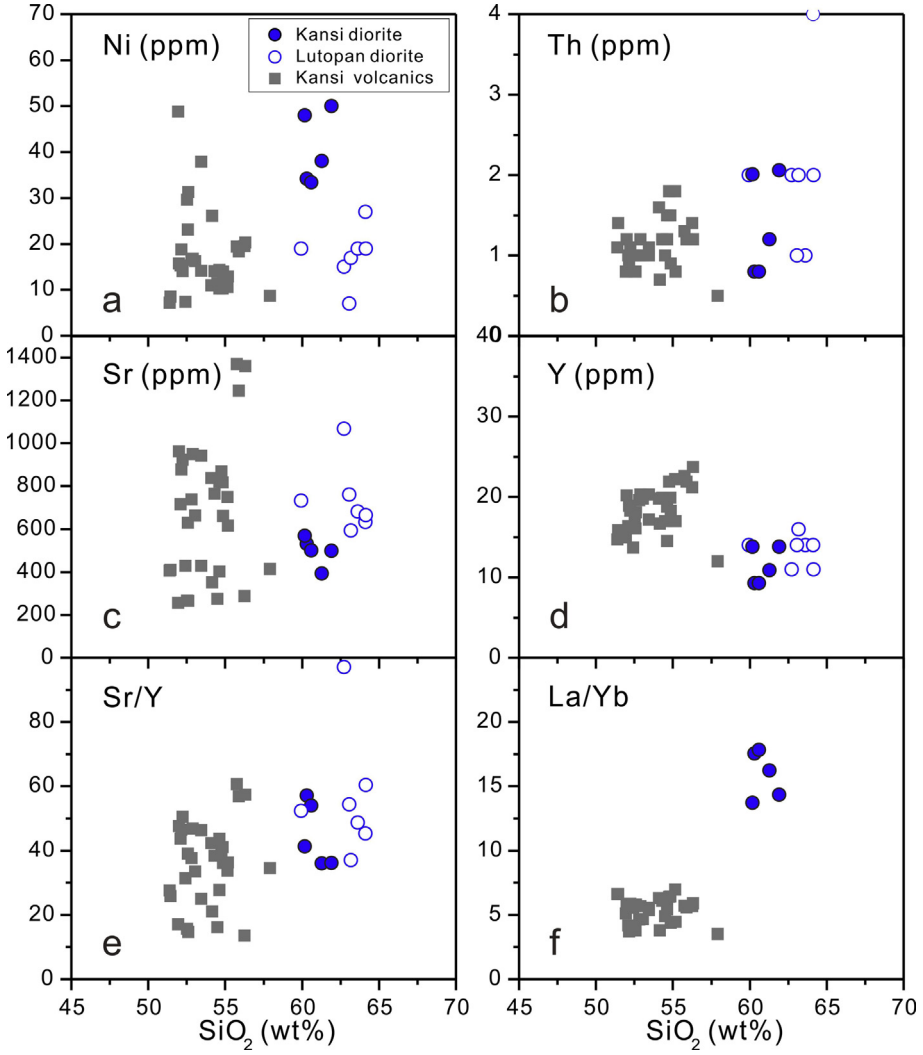

Fig. 14. Trace element variations with SiO_2 contents for Cebu adakites and arc volcanic rocks.

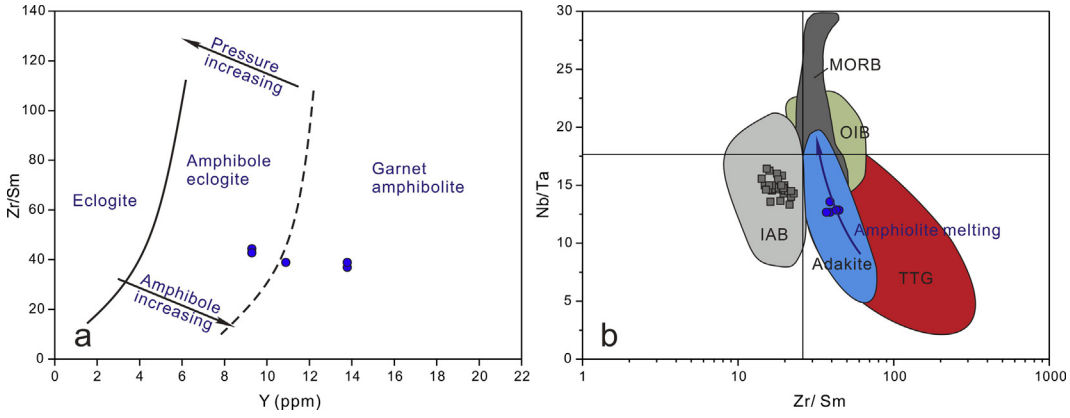

Fig. 15. Trace element diagrams for the Kansi diorites. a. Zr/Sm-Y diagram showing melting of subducted oceanic crust in the condition of amphibolite or eclogite. b. Nb/Ta-Zr/Sm diagram, after Foley et al. (2002).

(Gutscher et al., 2000; Peacock et al., 1994), highly oblique subduction (Yogodzinski et al., 1995), in slab windows where hot asthenosphere comes in direct contact with the plate edge during ridge subduction (Abratis and Worner, 2001; Thorkelson, 1996; Thorkelson and Breitsprecher, 2005) or tearing of a subducted slab (Yogodzinski et al., 2001), slab rollback (Wang et al., 2014; Wong et al., 2009), and slab detachment or break off (Gao et al., 2007; König et al., 2007; Omrani et al., 2008); (2) partial melting of previously formed garnet-bearing amphibolitic lower arc crust (Atherton and Petford, 1993; Chiaradia, 2009; Yumul et al., 2000a); (3) fractionation of garnet, hornblende ± titanite ± zircon from normal arc magmas under high or low pressure in the mantle

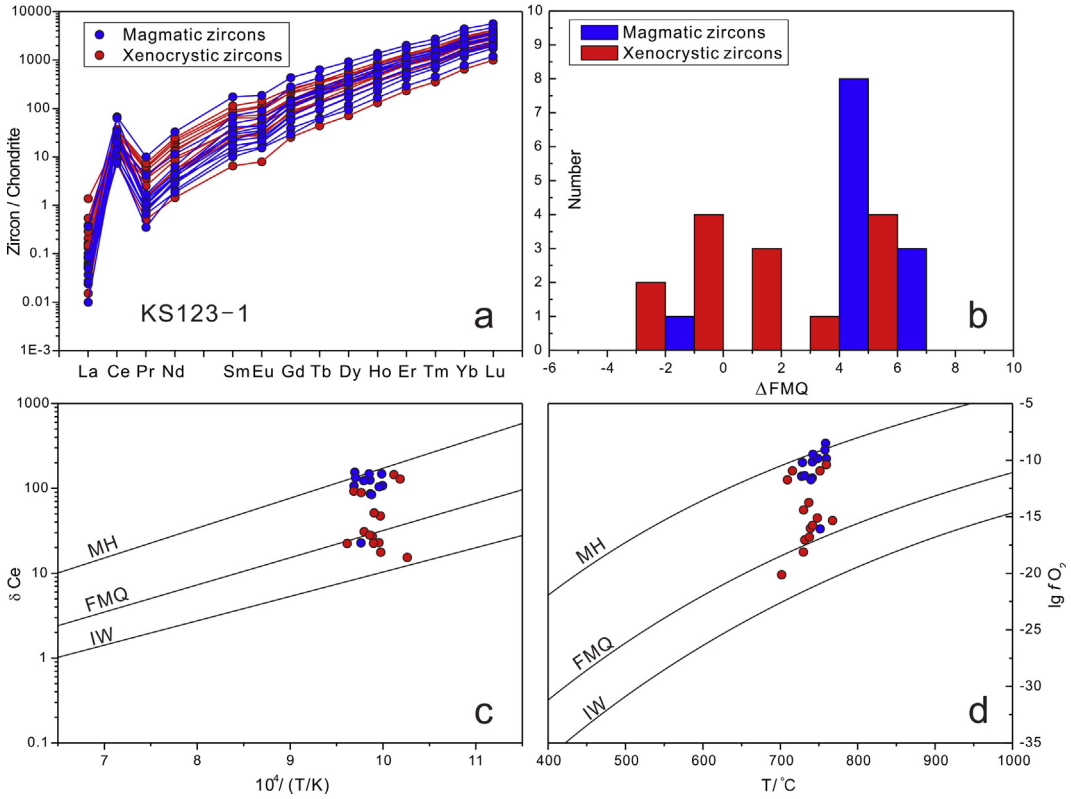

Fig. 16. Zircon trace elements showing the oxygen fugacities of the Kansi diorites. a. Chondrite normalized zircon trace element distribution diagram. b. Histogram of calculated ΔFMQ values for single zircons. c. Magma oxidation states for single zircons. d. Magma oxygen fugacities for single zircons. After Qiu et al. (2013).

Table 4
Zircon LA-MC-ICP-MS Lu-Hf isotopic copositions of the Kansi diorite, Cebu Island.

Sample No.	$^{176}Yb/^{177}Hf$	2σ	$^{176}Lu/^{177}Hf$	2σ	$^{176}Hf/^{177}Hf$	2σ	ε (0)	ε (t)	Age (Ma)	T_{DMI} (Ma)
Magmatic zircon										
KS123-1	0.073552	0.001489	0.001780	0.000037	0.283078	0.000014	10.8	13.0	106	251
KS123-2	0.058144	0.000675	0.001381	0.000018	0.283030	0.000015	9.1	11.4	111	318
KS123-4	0.059867	0.000535	0.001470	0.000011	0.283041	0.000014	9.5	11.8	111	303
KS123-5	0.054145	0.000616	0.001401	0.000019	0.283062	0.000016	10.3	12.6	113	272
KS123-6	0.086432	0.000259	0.002211	0.000018	0.283042	0.000018	9.5	11.8	112	308
KS123-7	0.034663	0.000378	0.001012	0.000014	0.283138	0.000019	12.9	15.2	108	160
KS123-8	0.049925	0.000232	0.001289	0.000008	0.283054	0.000014	10.0	12.4	114	282
KS123-10	0.034427	0.000125	0.000915	0.000002	0.283114	0.000015	12.1	14.5	111	194
KS123-14	0.076212	0.001130	0.002104	0.000031	0.282982	0.000017	7.4	9.8	113	394
KS123-23	0.098466	0.000717	0.002335	0.000012	0.283066	0.000019	10.4	12.7	112	273
KS123-25	0.051437	0.000581	0.001427	0.000008	0.282990	0.000020	7.7	10.0	109	376
KS123-27	0.076204	0.001096	0.002238	0.000033	0.283085	0.000029	11.1	13.3	107	244
Xenocrystic zircon										
KS123-3	0.072801	0.000152	0.001840	0.000004	0.282994	0.000015	7.8	10.3	116	374
KS123-9	0.080745	0.001006	0.002221	0.000018	0.282979	0.000016	7.3	9.9	125	400
KS123-12	0.069422	0.000979	0.001885	0.000037	0.282879	0.000024	3.8	6.2	116	541
KS123-13	0.081409	0.000472	0.002367	0.000013	0.282879	0.000033	3.8	6.1	113	550
KS123-15	0.063415	0.000300	0.001826	0.000008	0.282894	0.000025	4.3	6.8	121	519
KS123-16	0.038996	0.000130	0.001056	0.000004	0.283040	0.000017	9.5	11.9	116	301
KS123-17	0.087763	0.000274	0.002346	0.000008	0.282958	0.000015	6.6	8.9	116	433
KS123-18	0.056723	0.001096	0.001345	0.000020	0.283062	0.000018	10.3	12.8	120	272
KS123-20	0.048769	0.000514	0.001328	0.000026	0.283052	0.000014	9.9	12.4	118	286
KS123-24	0.053980	0.000582	0.001709	0.000015	0.282988	0.000020	7.6	10.1	120	382

or crust level (Castillo et al., 1999; Li et al., 2009; Macpherson et al., 2006; Richards, 2011; Richards and Kerrich, 2007).

As described in the zircon results above, there are a significant amount of xenocrystic zircon grains or zircon cores observed in the Kansi diorites (Fig. 10b), with zircon ages systematically older than the syn-magmatic zircons (Fig. 10c and d). The occurrence of xenocrystic zircon is a common feature of many igneous rocks, but there are some difficulties when one attempts to evaluate the origin of these xenocrystic cores (Corfu et al., 2003). These magmatic zircons may be from the mafic magma source during partial melting of the arc crust, or assimilation of the igneous or sedimentary crustal materials during magma ascent, or fractional crystallization in the magma chamber (AFC). The peak $^{206}Pb/^{238}U$ age (ca. 118 Ma) of these xenocrystic zircons is close to the zircon

Table 5
Whole rock Sr-Nd-Pb isotopic compositions of the Kansi diorites, Cebu Island.

Sr-Nd isotopes												
Sample No.	T (Ma)	$^{87}Sr/^{86}Sr$	1σ	Rb (ppm)	Sr (ppm)	$(^{87}Sr/^{86}Sr)i$	$^{143}Nd/^{144}Nd$	1σ	Sm (ppm)	Nd(ppm)	$(^{143}Nd/^{144}Nd)i$	εNd(t)
KS123-1	110	0.703207	0.000005	3.0	531	0.703181	0.512962	0.000002	3.38	17	0.512872	7.3
KS123-3	110	0.703240	0.000006	4.9	393	0.703183	0.512969	0.000003	3.78	18.7	0.512878	7.4
KS123-4	110	0.703175	0.000005	1.4	502	0.703163	0.512955	0.000002	3.4	17.2	0.512865	7.2
KS123-5	110	0.703226	0.000007	7.8	500	0.703155	0.512965	0.000002	4.3	23.4	0.512881	7.5
KS123-6	110	0.703205	0.000006	5.3	570	0.703163	0.512967	0.000002	4.5	23.1	0.512879	7.5
Pb isotopes												
Sample No.	T (Ma)	$^{206}Pb/^{204}Pb$		$^{207}Pb/^{204}Pb$		$^{208}Pb/^{204}Pb$	U(ppm)	Th (ppm)	Pb (ppm)	$^{206}Pb/^{204}Pbi$	$^{207}Pb/^{204}Pbi$	$^{208}Pb/^{204}Pbi$
KS123-1	110	18.561		15.523		38.176	0.4	0.8	3.5	18.437	15.517	38.094
KS123-3	110	18.759		15.548		38.398	0.4	1.2	2.1	18.550	15.538	38.192
KS123-4	110	18.595		15.538		38.247	0.4	0.8	3.5	18.471	15.532	38.165
KS123-5	110	18.515		15.580		38.429	0.7	2.1	3.7	18.320	15.571	38.228
KS123-6	110	18.591		15.519		38.186	0.7	2.0	3.6	18.388	15.509	37.986

ages of Kansi volcanics in the area (126–118 Ma, Deng et al., 2015), which have a basalt end-member. It means a newly underplated basaltic rock in the lower arc crust with composition equivalent to the Kansi volcanics could be the potential source of the Kansi adakites. Based on the previous studies, adakitic rocks which were proposed to be generated by partial melting of lower crust are mostly found in areas of thick continental or arc crust with thickness more than 30–35 km (Atherton and Petford, 1993; Chiaradia, 2009; Yumul et al., 2000a), and even thicker (≥50 km) in continental collision areas like in the Tibet and Dabie Mountain, China (Chung et al., 2003; Wang et al., 2007). Even the most recent experimental study of Qian and Hermann (2013) suggested the most appropriate P–T conditions for producing adakite/TTG from mafic lower crust are 800–950 °C and 10–12.5 kbar (corresponding to a depth of 30–40 km). Although the specific location of the Philippine archipelago in the Early Cretaceous is still not well constrained, it is believed that the Cebu Island and even the Philippine Mobile Belt were formed as an intra-oceanic island arc (Rangin et al., 1990), which could be in the interior of proto-PSP in the southern Pacific (Deng et al., 2015; Maruyama et al., 1989; Pubellier et al., 2003). We thus do not favor the genesis of lower crust melting considering the intra-oceanic island arc environment of the proto-PMB (Rangin et al., 1990), and there is no evidence that a thick lower arc crust existed in the area. Granted that partial melting of the lower arc crust happened, the generated adakitic magma would have systematically higher incompatible elements and lower compatible elements contents than the Kansi basalts. Nevertheless, it is not supported as their Ni and Th contents are mostly in the same range (Fig. 14a and b). The elevated Mg# of the Kansi and Lutopan diorites than those of the Kansi volcanics also excluded the petrogenesis of lower arc crust melting. Even though delamination melting of lower continental crust could generate high Mg# adakite like in the Dabie Mountain (Huang et al., 2008), it is not even practical in the intra-oceanic arc settings. The majority of these zircon xenocrysts occur as cores rimmed by narrow newly grown magmatic zircons, or simply as unrimmed subrounded or rarely euhedral crystals (Fig. 10b), but they have a magmatic origin as discriminated from their REE distribution patterns (Fig. 16a), high Th/U ratios (>0.6, Table 3) and consistent zircon U-Pb ages with the Kansi volcanics. Finally, the most likely scenario is that these zircons were from the Kansi volcanics in the strata which were intruded by the Kansi diorites, and were assimilated during ascent or late-stage crystallization of the adakitic magma, with too little time for corrosion or overgrowth.

For the genesis of fractionation of garnet, hornblende ± titanite ± zircon from normal arc magmas under high or low pressure in the mantle or crust level, a basaltic magma formed simultaneously with or earlier than the Kansi diorite is needed. As the only earlier formed basaltic rock which could be genetically related to the Kansi diorites in the area is the basalt of the Kansi volcanics (ca. 118 Ma, Deng et al., 2015), thus a basaltic magma with composition equivalent to the Kansi basalt stored in the shallow crust could be the only possible parental source of the Kansi diorites. If the Kansi diorites were generated from low pressure fractional crystallization of a basaltic magma which is equivalent to the Kansi basalt in composition, with hornblende± titanite± zircon in residue, a continuous and gradual variations of major and trace elements vs. SiO_2 contents from basaltic to dacitic compositions could be observed, with increasing incompatible elements, Sr/Y and La/Yb ratios, and decreasing MgO, Mg#, compatible elements, Y and Yb contents (Castillo et al., 1999; Richards and Kerrich, 2007). Nevertheless, the variation trend defined by Kansi and Lutopan diorites are distinct from those of the Kansi volcanic rocks on MgO contents, Mg# (Fig. 9), and trace element contents and ratios (Fig. 14), showing no genetic connections between these two types of rocks. Accordingly, the low pressure fractional crystallization model is not supported, and the low Y, Yb contents and high Sr/Y, La/Yb ratios of the Kansi and Lutopan diorites could reflect the features of primary adakitic magma. Thus, the only possible genesis of the Kansi diorites is slab melting plus mantle interaction during magma ascent, with minor assimilation of the Kansi volcanic rocks in the shallow crust during magma crystallization.

The Kansi diorites are depleted in HFSEs such as Nb, Ta and Ti, which is also the characteristics of arc volcanic rocks like Kansi volcanics (Fig. 7b). The genesis of HFSE depletion for normal island arc magma is still controversial, but mainly focused on the effect of Nb–Ta bearing residual minerals such as rutile, amphibole or Ti–Fe oxides like ilmenite and Ti-magnetite during slab dehydration or magma fractionation processes (Green and Pearson, 1987; Schmidt et al., 2004; Xiong et al., 2005). The generation of adakites could be analogous, as current model for producing adakites by partial melting of subducted oceanic crust requires garnet or amphibole in the residue to explain the low contents of Y, Yb and other HREEs, in the condition of eclogite or garnet amphibolite melting (Castillo, 2012; Defant and Drummond, 1990; Foley et al., 2002; Martin et al., 2005; Sen and Dunn, 1994), and the HFSE depletion of these adakites is generally interpreted as reflecting the residual behavior of minerals like rutile or amphibole during basalt melting (Foley et al., 2000, 2002; Green and Pearson, 1987). As shown on Fig. 15a, the Kansi diorites have moderate low Y concentrations, suggesting partial melting of the subducted oceanic crust in the P-T condition of garnet amphibolite to amphibole eclogite, which means both amphibole and garnet are the dominant residual minerals during partial melting. The low Nb/Ta and high Zr/Sm ratios of the Kansi adakites, similar to other adakites and TTGs worldwide, are also suggested to be caused by

amphibolite melting as shown by Fig. 15b, rather than eclogite melting (Foley et al., 2002). Although melting of rutile-bearing eclogite can explain the low HREE, HFSE concentrations and high Zr/Sm ratios, it produces high Nb/Ta ratio in coexisting melts. Finally, amphibolite melting of subducted oceanic crust could be the genesis of the Kansi diorites, as low Mg# amphiboles with Mg# below about 70 can significantly fractionate Nb from Ta, producing the required low Nb/Ta in coexisting melts (Foley et al., 2002).

5.3. Source of the Kansi diorites

There are systematic isotopic differences between MORBs from different ocean basins, reflecting some very large scale isotopic heterogeneities in the source mantle of these basalts (Hofmann, 2003). Although there are still more overlap in diagrams involving Sr-Nd isotopes (Fig. 12) and $^{207}Pb/^{204}Pb$ ratios (Fig. 13b), Indian Ocean MORBs have systematically lower ε_{Nd} values and consistently higher $^{208}Pb/^{204}Pb$ ratios than Pacific Ocean MORBs (Figs. 12 and 13a). The Sr-Nd-Hf isotopes of the Kansi diorites are highly depleted, close to the area of N-MORB (Figs. 11 and 12), indicating a juvenile oceanic crust as the source. The Hf isotopes of the comagmatic zircons are close to the Kansi volcanics and Amami plateau basalts and tonalites, much lower than the Huatung basin gabbro and diabase (Fig. 11), which have been proposed as an Early Cretaceous fragment of trapped Indian-type MORB in the West Philippine Basin (WPB) (Hickey-Vargas et al., 2008). Besides, Sr-Nd-Pb isotope compositions of the Kansi diorites are also close to the range of Amami Plateau basalts and tonalites, projected in the area between Pacific-type and Indian-type MORB (Figs. 12 and 13), even much closer to the area of Pacific-MORB. As proposed by Hickey-Vargas et al. (2008), the Sr, Nd, Pb and Hf isotopic results of the Amami plateau basalts and tonalites indicate that the pre-subduction mantle wedge involved in the generation at 115 Ma was of Pacific-MORB to transitional Indian-MORB isotopic characteristics. They further suggest that the subduction components of the Amami Plateau rocks were derived from clay-rich pelagic sediments and relatively unaltered Pacific-type MORB. However, the higher $\varepsilon_{Nd}(t)$ values of the Kansi diorites than the lower limit of the Pacific-MORB (Fig. 12), combining with Pacific-MORB range $(^{207}Pb/^{204}Pb)_i$ values (Fig. 13b) indicate the insignificant involvement of pelagic sediments in the source. Alternatively, it may represent influences from the Neotethys plate subduction (Sun, 2016; Zhang et al., 2017b). Initial $^{87}Sr/^{86}Sr$ ratios for the Kansi diorites are higher than those of the Pacific-MORB and Amami Plateau rocks, which may be due to incorrect age correction caused by Rb loss during hydrothermal alteration, as the diorites are altered during mineralization stage, followed by loss of immobile elements such as Rb and Sr as discussed above. Therefore, we propose that the Kansi diorites were generated from partial melting of a Pacific-type MORB, with insignificant pelagic sediments involved in the source.

5.4. Implications for Cu-Au mineralization

Adakites from the circum-Pacific have strong connections to Cu deposits (Aguillon-Robles et al., 2001; Cooke et al., 2005; Kay et al., 1999; Oyarzun et al., 2001, 2002; Reich et al., 2003; Sajona and Maury, 1998; Sun et al., 2010), and the close genetic association between porphyry Cu-Au deposits and adakites has been proposed for more than a decade (Chiaradia et al., 2012; Deng et al., 2016; Mungall, 2002; Richards, 2011; Sillitoe, 2010; Sun et al., 2011, 2012, 2015, 2017; Thieblemont et al., 1997; Zhang et al., 2017a). In places where adakites coexist with non-adakitic igneous rocks, mineralization is usually associated with the adakites (Reich et al., 2003; Sun et al., 2011, 2012; Thieblemont et al., 1997). This model has also been supported by the work of Sajona and Maury (1998), where they proposed that most of the porphyry Cu and epithermal Au deposits in the Philippines are spatially and temporally related to adakites.

As we know, copper is a moderately incompatible chalcophile element, and its behavior is strongly controlled by sulfides (Sun et al., 2011, 2015). The speciation of sulfur is controlled by oxygen fugacity (Sun et al., 2004). It has been further argued that adakites derived by slab melting have high oxygen fugacities, which may eliminate sulfide in the source region and keep the melt sulfide under-saturated, and thereby promoting porphyry Cu-Au mineralization (Ballard et al., 2002; Deng et al., 2016; Kelley and Cottrell, 2009; Mungall, 2002; Oyarzun et al., 2001; Sun et al., 2013; Wang et al., 2013; Zhang et al., 2017a; Zhang et al., 2013). As mid-ocean ridge basalt (MORB) has Cu contents of ~100 ppm (Sun et al., 2003), which is more than three times higher than those of the primitive mantle and the continental crust (McDonough and Sun, 1995; Rudnick and Gao, 2003), partial melting of subducted young oceanic slabs at oxygen fugacities > ΔFMQ +1.5 ~ +2 (the critical number for porphyry Cu-Au mineralization, corresponding to Fe^{3+}/total Fe ratio of ~0.2) (Sun et al., 2016, 2017; Zhang et al., 2017a), forms magmas with high initial Cu contents (>500 ppm), which may easily reach industrial Cu contents for porphyry deposit (Sun et al., 2017).

Zircon is a resistant mineral with high closure temperature. It incorporated Ce^{4+} and thus the oxygen fugacities calculated from the Ce enrichment can provide a qualitative estimate of the oxidation state of the magma (Trail et al., 2011). The high oxygen fugacities of the Kansi diorites reflected by magmatic zircons are much higher than ΔFMQ +2 (Fig. 16b), and closed to the hematite–magnetite oxygen fugacity (HM) buffer (Fig. 16c and d), similar to the oxygen fugacities of most of the porphyry deposits worldwide (Sun et al., 2015). Given the oceanic crust have higher initial Cu contents than the continental crust and mantle, the oceanic slab derived Kansi diorites with high oxygen fugacities are thus favorable for Cu mineralization.

As we discussed above, the Kansi diorites have geochemical similarities with the ore-bearing Lutopan diorites in the large Atlas porphyry Cu-Au deposit, indicating a similar magma genesis, further suggesting they may be genetically related, or even as two branches of magma from a single deep magma chamber. Considering the similarities in geological settings of the Kansi region and the Atlas large Cu-Au deposit in the Cebu Island (i.e., contemporary ore-bearing adakitic diorites intrude into the earlier Cansi Formation volcanics), combining with the porphyry-type alteration features (including argillic, chloritic, siliceous, and occasionally potassic alteration), and common Cu mineralization (veins or disseminated pyrite, chalcopyrite and bornite, and supergene malachite) in the Kansi area, we propose there could be a good potential for porphyry Cu-Au deposit exploration in the Kansi area. More exploration work is still needed.

5.5. Tectonic implications

The location and tectonic setting of the Philippine archipelago in the Mesozoic are still not well constrained, although the Mesozoic evolution of the Sundaland and Southeast Asia has been reconstructed by many authors (Hall, 2012; Hall et al., 2009; Metcalfe, 2006, 2011; Zhou et al., 2008). As proposed by previous workers, the Early Cretaceous Amami Plateau basalt and tonalite in the northern WPB, the Huatung basin gabbro in the western WPB, Early Cretaceous Cebu arc volcanic suites and other ophiolitic complexes in the central Philippines were possibly formed on a Jurassic-Paleocene island arc terrane in the domain of proto-PSP, which have been separated by the opening of WPB from the Eocene (Deng et al., 2015; Deschamps et al., 2000; Hickey-Vargas et al.,

2008). According to the present hypothesis, the position of the Philippines before the opening of WPB in the Eocene must have been in the southern Pacific, or at the boundary between the Pacific and North New Guinea Basin (Maruyama et al., 1989), which was opened as a back-arc basin along the northern margin of Australia during the Middle Jurassic-Early Cretaceous (Monnier et al., 1995; Pubellier et al., 2003). The New Guinea and Huatung Basins could both be parts of a single plate: the proto-PSP, similar to the current situation of the back-arc basins of the PSP (Deschamps and Lallemand, 2002). The proto-PSP must have spanned from the low latitudes of the southern to the northern hemispheres to explain the contrasting paleo-geographic locations of the Huatung and New Guinea basins (Deschamps and Lallemand, 2002).

Based on the present hypothesis that Huatung basin was a part of the proto-PSP, the lithosphere of proto-PSP might be Indian-MORB type as indicated by the Indian-type feature of Huatung basin (Deng et al., 2015). This is also supported by the widely development of Indian-type Eocene basalt in the principal part of WPB, which is proposed to have opened in the domain of proto-PSP (Hall, 2001; Hall et al., 1995; Rangin et al., 1990). Nevertheless, the Pacific-type Sr-Nd-Pb-Hf isotopes features of the Kansi diorites, which are quite different from the Huatung Basin gabbros, indicate a dominant input of paleo-Pacific Plate materials during slab melting in the Early Cretaceous. Considering the geodynamic history of paleo-Pacific Plate and proto-PSP in the Mesozoic (Hall, 2012; Hall et al., 2009; Maruyama et al., 1997; Zhou et al., 2008), the Early Cretaceous island arc rocks and ophiolite complexes in the central Philippines were proposed to be related to the subduction and rollback of paleo-Pacific Plate to the proto-PSP and Australian margin at ca. 126 Ma prior to the opening of the WPB in the Eocene (Deng et al., 2015),

The widely developed normal arc volcanic rocks in the Cebu Island from ca. 126–115 Ma suggested ca. 10 Myrs of mantle melting caused by subduction and dehydration of paleo-Pacific Plate (Deng et al., 2015). The absence of adakites generated during this period have ruled out slab melting, suggesting the subducted paleo-Pacific Plate in the area might be old and cool, and could not reach the P-T condition of slab melting, as the slab melting process is believed to require an exceptionally high temperature environment. Thus a high thermal flow is needed for generating adakite from partial melting of the paleo-Pacific Plate at ca. 110 Ma. It is widely accepted that back-arc basins at convergent plate boundaries are produced by the rollback of subducted plates in response to the interplay between the convergence of tectonic plates and the velocity of subduction. In fact, initial widespread extension along the eastern margin of Australia and in the New Zealand region started in the Early to Middle Cretaceous, and volcanic sediments were deposited along the East Australian margin in the Early Cretaceous (Barremian–Albian) (Bryan et al., 1997), and have been interpreted to have resulted from widespread backarc extension caused by east to northeast-directed rollback of a west to southwest-dipping subduction (Betts et al., 2002; Forster and Lister, 2003; Schellart et al., 2006; Veevers, 2000). Slab rollback provides the conditions for the upwelling of the hot asthenosphere, causing a thermal anomaly and the subsequent partial melting of the subducted slab. Finally, the ca. 110 Ma adakites developed in the Kansi area and the Atlas mining district might have been generated by partial melting of the subducted slab during the slab rollback process.

6. Conclusions

Combined with the comprehensive geochronological and geochemical studies on the Kansi and Lutopan diorites in the Cebu Island, central Philippines, we draw the following conclusions:

(1) The age of formation for the Kansi diorite is ca. 110 Ma in the Early Cretaceous, close to the age of Lutopan diorites in the Atlas porphyry Cu-Au deposit, and younger than the Cebu Island volcanic suites.
(2) The Kansi and Lutopan diorites in the Cebu Island are both high-Mg adakites, generated by partial melting of the subducted paleo-Pacific Plate beneath the proto-PSP, followed by a certain degree of mantle interaction and crustal contamination.
(3) The Kansi diorites are characterized by high oxygen fugacities, thus having a good potential for the exploration of porphyry Cu-Au deposit.
(4) The successive formation of normal arc volcanics and adakites in the Cebu Island are probably related to the subduction and rollback of paleo-Pacific Plate to the proto-PSP in the Early Cretaceous.

Acknowledgements

This study is supported by the National Natural Science Foundation of China (Nos. 91328204, 41673040, 41373007), the DREAM project of MOST China (No. 2016YFC0600404), and China Postdoctoral Science Foundation (2015M582003). We wish to thank Mr. J. Zhang from CNMC (Phils.) and Dr. Al Emil G. Berador from Geosciences Division, MGB-7, Cebu, Philippines for the assistance in the field. Dr. Franco Pirajno and two anonymous reviewers are greatly appreciated for English polishing and constructive review comments, which have significantly improved the manuscript.

Appendix A. Supplementary data

Supplementary data associated with this article can be found, in the online version, at http://dx.doi.org/10.1016/j.oregeorev.2017.05.006.

References

Abratis, M., Worner, G., 2001. Ridge collision, slab-window formation, and the flux of Pacific asthenosphere into the Caribbean realm. Geology 29, 127–130.
Aguillon-Robles, A., Calmus, T., Benoit, M., Bellon, H., Maury, R.O., Cotten, J., Bourgois, J., Michaud, F., 2001. Late miocene adakites and Nb-enriched basalts from Vizcaino Peninsula, Mexico: indicators of East Pacific Rise subduction below Southern Baja California? Geology 29, 531–534.
Atherton, M.P., Petford, N., 1993. Generation of sodium-rich magmas from newly underplated basaltic crust. Nature 362, 144–146.
Aurelio, M.A., 2000. Shear partitioning in the Philippines: constraints from Philippine Fault and global positioning system data. Island Arc 9, 584–597.
Aurelio, M.A., Peña, R.E., 2002. Geology and Mineral Resources of the Philippines – Volume 1: Geology. Department of Environment and Natural Resources-Mines and Geosciences Bureau, p. 391.
Aurelio, M.A., Peña, R.E., 2010. Geology of the Philippines. Mines and Geosciences Bureau, Quezon City, pp. 1–532.
Aurelio, M.A., Pena, R.E., Taguibao, K.J.L., 2013. Sculpting the Philippine archipelago since the Cretaceous through rifting, oceanic spreading, subduction, obduction, collision and strike-slip faulting: contribution to IGMA5000. J. Asian Earth Sci. 72, 102–107.
Balce, G.R., 1970. An Introduction to the Stratigraphy of Cebu. Bureau of Mines (unpublished).
Ballard, J.R., Palin, M.J., Campbell, I.H., 2002. Relative oxidation states of magmas inferred from Ce(IV)/Ce(III) in zircon: application to porphyry copper deposits of northern Chile. Contrib. Miner. Petrol. 144, 347–364.
Bellon, H., Yumul, G.P., 2001. Miocene to Quaternary adakites and related rocks in Western Philippine arc sequences. Compt. Rend. Acad. Sci. Ser. Fasc. Sci. Terre Et Des Planet. 333, 343–350.
Betts, P.G., Giles, D., Lister, G.S., Frick, L.R., 2002. Evolution of the Australian lithosphere. Aust. J. Earth Sci. 49, 661–695.
Bourdon, E., Eissen, J.P., Gutscher, M.A., Monzier, M., Samaniego, P., Robin, C., Bollinger, C., Cotten, J., 2002. Slab melting and slab melt metasomatism in the Northern Andean Volcanic Zone: adakites and high-Mg andesites from Pichincha volcano (Ecuador). Bull. Soc. Geol. Fr. 173, 195–206.
Bouvier, A., Vervoort, J.D., Patchett, P.J., 2008. The Lu–Hf and Sm–Nd isotopic composition of CHUR: constraints from unequilibrated chondrites and

implications for the bulk composition of terrestrial planets. Earth Planet. Sci. Lett. 273, 48–57.
Bryan, S.E., Constantine, A.E., Stephens, C.J., Ewart, A., Schön, R.W., Parianos, J., 1997. Early Cretaceous volcano-sedimentary successions along the eastern Australian continental margin: implications for the break-up of eastern Gondwana. Earth Planet. Sci. Lett. 153, 85–102.
Castillo, P.R., 2012. Adakite petrogenesis. Lithos 134, 304–316.
Castillo, P.R., Janney, P.E., Solidum, R.U., 1999. Petrology and geochemistry of Camiguin Island, southern Philippines: insights to the source of adakites and other lavas in a complex arc setting. Contrib. Miner. Petrol. 134, 33–51.
Castillo, P.R., Rigby, S.J., Solidum, R.U., 2007. Origin of high field strength element enrichment in volcanic arcs: geochemical evidence from the Sulu Arc, southern Philippines. Lithos 97, 271–288.
Chiaradia, M., 2009. Adakite-like magmas from fractional crystallization and melting-assimilation of mafic lower crust (Eocene Macuchi arc, Western Cordillera, Ecuador). Chem. Geol. 265, 468–487.
Chiaradia, M., Müntener, O., Beate, B., Fontignie, D., 2009. Adakite-like volcanism of Ecuador: lower crust magmatic evolution and recycling. Contrib. Miner. Petrol. 158, 563–588.
Chiaradia, M., Ulianov, A., Kouzmanov, K., Beate, B., 2012. Why large porphyry Cu deposits like high Sr/Y magmas? Sci. Rep. 2, 685.
Chung, S.L., Liu, D.Y., Ji, J.Q., Chu, M.F., Lee, H.Y., Wen, D.J., Lo, C.H., Lee, T.Y., Qian, Q., Zhang, Q., 2003. Adakites from continental collision zones: melting of thickened lower crust beneath southern Tibet. Geology 31, 1021–1024.
Cooke, D.R., Hollings, P., Walshe, J.L., 2005. Giant porphyry deposits: characteristics, distribution, and tectonic controls. Econ. Geol. 100, 801–818.
Corfu, F., Hanchar, J.M., Hoskin, P.W., Kinny, P., 2003. Atlas of zircon textures. Rev. Mineral. Geochem. 53, 469–500.
Defant, M.J., Drummond, M.S., 1990. Derivation of some modern arc magmas by melting of young subducted lithosphere. Nature 347, 662–665.
Defant, M.J., Kepezhinskas, P., 2001. Evidence suggests slab melting in arc magmas. EOS Trans. 82. 65-65.
Deng, J.H., Yang, X.Y., Zhang, Z.-F., Santosh, M., 2015. Early Cretaceous arc volcanic suite in Cebu Island, Central Philippines and its implications on paleo-Pacific plate subduction: constraints from geochemistry, zircon U-Pb geochronology and Lu–Hf isotopes. Lithos 230, 166–179.
Deng, J.H., Yang, X.Y., Li, S., Gu, H.L., Mastoi, A.S., Sun, W.D., 2016. Partial melting of subducted paleo-Pacific plate during the early Cretaceous: constraint from adakitic rocks in the Shaxi porphyry Cu-Au deposit, Lower Yangtze River Belt. Lithos 262, 651–667.
Deschamps, A., Lallemand, S., 2002. The West Philippine Basin: an Eocene to early Oligocene back arc basin opened between two opposed subduction zones. J. Geophys. Res. 107, 2322.
Deschamps, A., Monie, P., Lallemand, S., Hsu, S.K., Yeh, K.Y., 2000. Evidence for Early Cretaceous oceanic crust trapped in the Philippine Sea Plate. Earth Planet. Sci. Lett. 179, 503–516.
Dimalanta, C.B., Yumul, G.P., 2006. Magmatic and amagmatic contributions to crustal growth in the Philippine island arc system: comparison of the Cretaceous and post-Cretaceous periods. Geosci. J. 10, 321–329.
Dimalanta, C.B., Suerte, L.O., Yumul, G.P., Tamayo, R.A., Ramos, E.G.L., 2006. A Cretaceous supra-subduction oceanic basin source for Central Philippine ophiolitic basement complexes: geological and geophysical constraints. Geosci. J. 10, 305–320.
Drummond, M.S., Defant, M.J., Kepezhinskas, P.K., 1996. Petrogenesis of slab-derived trondhjemite-tonalite-dacite/adakite magmas. Trans. R. Soc. Edinburgh Earth Sci. 87, 205–215.
Faure, M., Marchadier, Y., Rangin, C., 1989. Pre-eocene synmetamorphic structure in the Mindoro-Romblon-Palawan Area, West Philippines, and implications for the History of Southeast-Asia. Tectonics 8, 963–979.
Foley, S.F., Barth, M.G., Jenner, G.A., 2000. Rutile/melt partition coefficients for trace elements and an assessment of the influence of rutile on the trace element characteristics of subduction zone magmas. Geochim. Cosmochim. Acta 64, 933–938.
Foley, S., Tiepolo, M., Vannucci, R., 2002. Growth of early continental crust controlled by melting of amphibolite in subduction zones. Nature 417, 837–840.
Forster, M.A., Lister, G.S., 2003. Cretaceous metamorphic core complexes in the Otago Schist, New Zealand. Aust. J. Earth Sci. 50, 181–198.
Gao, Y.F., Hou, Z.Q., Kamber, B.S., Wei, R.H., Meng, X.J., Zhao, R.S., 2007. Adakite-like porphyries from the southern Tibetan continental collision zones: evidence for slab melt metasomatism. Contrib. Miner. Petrol. 153, 105–120.
Geng, J.Z., Li, H.K., Zhang, J., Zhou, H.Y., Li, H.M., 2011. Zircon Hf isotope analysis by means of LA-MC-ICP-MS. Geol. Bull. China 30, 1508–1513 (in Chinese with English abstract).
Gervasio, F., 1971. Geotectonic development of the Philippines. J. Geol. Soc. Philippines 25, 18–38.
Gonzalez-Partida, E., Levresse, G., Carrillo-Chavez, A., Cheilletz, A., Gasquet, D., Jones, D., 2003. Paleocene adakite Au-Fe bearing rocks, Mezcala, Mexico: evidence from geochemical characteristics. J. Geochem. Explor. 80, 25–40.
Green, T.H., Pearson, N.J., 1987. An experimental study of Nb and Ta partitioning between Ti-rich minerals and silicate liquids at high pressure and temperature. Geochim. Cosmochim. Acta 51, 55–62.
Gregoire, M., Jego, S., Maury, R.C., Polve, M., Payot, B., Tamayo, R.A., Yumul, G.P., 2008. Metasomatic interactions between slab-derived melts and depleted mantle: insights from xenoliths within Monglo adakite (Luzon arc, Philippines). Lithos 103, 415–430.
Griffin, W.L., Pearson, N.J., Belousova, E., Jackson, S.E., van Achterbergh, E., O'Reilly, S.Y., Shee, S.R., 2000. The Hf isotope composition of cratonic mantle: LAM-MC-ICPMS analysis of zircon megacrysts in kimberlites. Geochim. Cosmochim. Acta 64, 133–147.
Gu, H.-O., Xiao, Y., Santosh, M., Li, W.-Y., Yang, X., Pack, A., Hou, Z., 2013. Spatial and temporal distribution of Mesozoic adakitic rocks along the Tan-Lu fault, Eastern China: constraints on the initiation of lithospheric thinning. Lithos 177, 352–365.
Gutscher, M.A., Maury, R., Eissen, J.P., Bourdon, E., 2000. Can slab melting be caused by flat subduction? Geology 28, 535–538.
Hall, R., 2001. Cenozoic reconstructions of SE Asia and the SW Pacific: Changing patterns of land and sea. In: Metcalfe, I., Smith, J.M.B., Morwood, M., Davidson, I. D. (Eds.), Faunal and Floral Migrations and Evolution in Se Asia-Australasia. A.A. Balkema (Swets & Zeitlinger Publishers), Lisse, pp. 35–56.
Hall, R., 2012. Late Jurassic-Cenozoic reconstructions of the Indonesian region and the Indian Ocean. Tectonophysics 570, 1–41.
Hall, R., Ali, J.R., Anderson, C.D., Baker, S.J., 1995. Origin and motion history of the Philippine Sea Plate. Tectonophysics 251, 229–250.
Hall, R., Clements, B., Smyth, H.R., 2009. Sundaland: basement character, structure and plate tectonic development. In: Proceedings Indonesian Petroleum Association, 33rd Annual Convention, IPA09-G-134, pp. 1–27.
Hastie, A.R., Kerr, A.C., Pearce, J.A., Mitchell, S.F., 2007. Classification of altered volcanic island arc rocks using immobile trace elements: development of the Th-Co discrimination diagram. J. Petrol. 48, 2341–2357.
He, X., Zhu, X., Yang, C., Tang, S., 2005. High-precision analysis of Pb isotope ratios using MC-ICP-MS. Acta Geosci. Sin. 26, 19–22 (in Chinese with English abstract).
Hickey-Vargas, R., Bizimis, M., Deschamps, A., 2008. Onset of the Indian Ocean isotopic signature in the Philippine Sea plate: Hf and Pb isotope evidence from Early Cretaceous terranes. Earth Planet. Sci. Lett. 268, 255–267.
Hofmann, A.W., 2003. Sampling mantle heterogeneity through oceanic basalts: isotopes and trace elements. Treatise Geochem. 2, 61–101.
Huang, F., Li, S.G., Dong, F., He, Y.S., Chen, F.K., 2008. High-Mg adakitic rocks in the Dabie orogen, central China: implications for foundering mechanism of lower continental crust. Chem. Geol. 255, 1–13.
Jego, S., Maury, R.C., Polve, M., Yumul, G.P., Bellon, H., Tamayo, R.A., Cotten, J., 2005. Geochemistry of adakites from the Philippines: constraints on their origins. Resour. Geol. 55, 163–187.
Kay, R.W., 1978. Aleutian magnesian andesites: melts from subducted Pacific Ocean crust. J. Volcanol. Geoth. Res. 4, 117–132.
Kay, S.M., Mpodozis, C., Coira, B., 1999. Neogene magmatism, tectonism, and mineral deposits of the Central Andes (22 to 33 S latitude). In: Skinner, B.J. (Ed.), Geology and Ore Deposits of the Central Andes. Society of Economic Geologists, Special Publication, pp. 27–59.
Kelemen, P.B., 1995. Genesis of high Mg# andesites and the continental crust. Contrib. Miner. Petrol. 120, 1–19.
Kelley, K.A., Cottrell, E., 2009. Water and the oxidation state of subduction zone magmas. Science 325, 605–607.
Kepezhinskas, P.K., Defant, M.J., Drummond, M.S., 1995. Na metasomatism in the island-arc mantle by slab melt—peridotite interaction: evidence from mantle xenoliths in the North Kamchatka Arc. J. Petrol. 36, 1505–1527.
Kerntke, M., 1992. Petrographic, geochemical and geochronologic investigation of the porphyry-copper deposit Atlas-Mining on Cebu Island (Philippines). PhD. thesis. <www.dr-kerntke.de/html/body_abstract_2.html>.
Kerntke, M., Tarkian, M., Baumann, A., 1991. Geochemie und Geochronologie der Magmatite von Lutopan und Talamban, Cebu (Philippinen). Mitt. Geol.-Paläont. Inst. Univ. Hamburg 71, 93–120 (in German).
König, S., Schuth, S., Münker, C., Qopoto, C., 2007. The role of slab melting in the petrogenesis of high-Mg andesites: evidence from Simbo Volcano, Solomon Islands. Contrib. Miner. Petrol. 153, 85–103.
Li, J.-W., Zhao, X.-F., Zhou, M.-F., Ma, C.-Q., Souza, Z.S., Vasconcelos, P., 2009. Late Mesozoic magmatism from the Daye region, eastern China: U-Pb ages, petrogenesis, and geodynamic implications. Contrib. Miner. Petrol. 157, 383–409.
Liang, X., Wei, G., Li, X., Liu, Y., 2003. Precise measurement of 143Nd/144Nd and Sm/Nd ratios using multiple-collectors inductively coupled plasma-mass spectrometer (MC-ICPMS). Geochimica 32, 91–96 (in Chinese with English abstract).
Liang, J.L., Ding, X., Sun, X.M., Zhang, Z.M., Zhang, H., Sun, W.D., 2009. Nb/Ta fractionation observed in eclogites from the Chinese Continental Scientific Drilling Project. Chem. Geol. 268, 27–40.
Lin, J., Liu, Y., Yang, Y., Hu, Z., 2016. Calibration and correction of LA-ICP-MS and LA-MC-ICP-MS analyses for element contents and isotopic ratios. Solid Earth Sci. 1, 5–27.
Liu, Y., Liu, H.C., Li, X.H., 1996. Simultaneous and precise determination of 40 trace elements in rock samples using ICP-MS. Geochimica 25, 552–558.
Liu, Y.S., Hu, Z.C., Gao, S., Günther, D., Xu, J., Gao, C.G., Chen, H.H., 2008. In situ analysis of major and trace elements of anhydrous minerals by LA-ICP-MS without applying an internal standard. Chem. Geol. 257, 34–43.
Liu, Y., Hu, Z., Zong, K., Gao, C., Gao, S., Xu, J., Chen, H., 2010. Reappraisement and refinement of zircon U-Pb isotope and trace element analyses by LA-ICP-MS. Chin. Sci. Bull. 55, 1535–1546.
Ludwig, K.R., 2003. ISOPLOT 3.00: A Geochronological Toolkit for Microsoft Excel. Berkeley Geochronology Center, California, Berkeley, pp. 1–39.
Machado, N., Simonetti, A., 2001. U-Pb dating and Hf isotopic composition of zircon by laser ablation MC-ICP-MS. In: Sylvester, P. (Ed.), Laser-Ablation-ICPMS in the

Earth Sciences: Principles and Applications: Short Course of Mineralogical Association of Canada 29.
Macpherson, C.G., Dreher, S.T., Thirlwall, M.F., 2006. Adakites without slab melting: High pressure differentiation of island arc magma, Mindanao, the Philippines. Earth Planet. Sci. Lett. 243, 581–593.
Martin, H., Smithies, R.H., Rapp, R., Moyen, J.F., Champion, D., 2005. An overview of adakite, tonalite-trondhjemite-granodiorite (TTG), and sanukitoid: relationships and some implications for crustal evolution. Lithos 79, 1–24.
Maruyama, S., Liou, J.G., Seno, T., 1989. Mesozoic and Cenozoic evolution of Asia. In: Ben-Avraham, Z. (Ed.), The Evolution of the Pacific Ocean Margin. Oxf. Monogr. Geol. Geophys., pp. 75–99.
Maruyama, S., Isozaki, Y., Kimura, G., 1997. Paleogeographic maps of the Japanese Islands: plate tectonic synthesis from 750 Ma to the present. Island Arc 6, 121–142.
Maury, R.C., Sajona, F.G., Pubellier, M., Bellon, H., Defant, M.J., 1996. Fusion de la croute oceanique dans les zones de subduction/collision recentes; l'exemple de Mindanao (Philippines). Bull. Soc. Geol. Fr. 167, 579–595.
McDonough, W., Sun, S., 1995. The composition of the Earth. Chem. Geol. 120, 223–253.
Metcalfe, I., 2006. Paleozoic and Mesozoic tectonic evolution and palaeogeography of East Asian crustal fragments: the Korean Peninsula in context. Gondwana Res. 9, 24–46.
Metcalfe, I., 2011. Tectonic framework and Phanerozoic evolution of Sundaland. Gondwana Res. 19, 3–21.
Mitchell, A.G.H., Hernandez, F., dela Cruz, A.P., 1986. Cenozoic evolution of the Philippine archipelago. J. SE Asian Earth Sci. 1, 2–33.
MMAJ-JICA, 1990. Consolidated report on Cebu-Bohol-Southwest Leyte Area. The Mineral Exploration - Mineral Deposits and Tectonics of Two Contrasting Environments in the Republic of the Philippines.
Monnier, C., Girardeau, J., Maury, R.C., Cotten, J., 1995. Back-Arc Basin Origin for the East Sulawesi Ophiolite (Eastern Indonesia). Geology 23, 851–854.
Moyen, J.F., 2009. High Sr/Y and La/Yb ratios: the meaning of the "adakitic signature". Lithos 112, 556–574.
Mungall, J.E., 2002. Roasting the mantle: slab melting and the genesis of major Au and Au-rich Cu deposits. Geology 30, 915–918.
Nowell, G.M., Kempton, P.D., Noble, S.R., Fitton, J.G., Saunders, A.D., Mahoney, J.J., Taylor, R.N., 1998. High precision Hf isotope measurements of MORB and OIB by thermal ionisation mass spectrometry: insights into the depleted mantle. Chem. Geol. 149, 211–233.
Omrani, J., Agard, P., Whitechurch, H., Benoit, M., Prouteau, G., Jolivet, L., 2008. Arc-magmatism and subduction history beneath the Zagros Mountains, Iran: a new report of adakites and geodynamic consequences. Lithos 106, 380–398.
Oyarzun, R., Marquez, A., Lillo, J., Lopez, I., Rivera, S., 2001. Giant versus small porphyry copper deposits of Cenozoic age in northern Chile: adakitic versus normal calc-alkaline magmatism. Miner. Depos. 36, 794–798.
Oyarzun, R., Marquez, A., Lillo, J., Lopez, I., Rivera, S., 2002. Reply to Discussion on "Giant versus small porphyry copper deposits of Cenozoic age in northern Chile: adakitic versus normal calc-alkaline magmatism" by Oyarzun R, Marquez A, Lillo J, Lopez I, Rivera S (Mineralium Deposita 36: 794–798, 2001). Miner. Depos. 37, 795–799.
Ozawa, A., Tagami, T., Listanco, E.L., Arpa, C.B., Sudo, M., 2004. Initiation and propagation of subduction along the Philippine Trench: evidence from the temporal and spatial distribution of volcanoes. J. Asian Earth Sci. 23, 105–111.
Peacock, S.M., Rushmer, T., Thompson, A.B., 1994. Partial melting of subducting oceanic crust. Earth Planet. Sci. Lett. 121, 227–244.
Pearce, J.A., 1982. Trace element characteristics of lavas from destructive plate boundaries. In: Thorpe, R.S. (Ed.), Andesites. JohnWiley, Chichester, pp. 525–547.
Pubellier, M., Ali, J., Monnier, C., 2003. Cenozoic plate interaction of the Australia and Philippine Sea Plates: "hit-and-run" tectonics. Tectonophysics 363, 181–199.
Qian, Q., Hermann, J., 2013. Partial melting of lower crust at 10–15 kbar: constraints on adakite and TTG formation. Contrib. Miner. Petrol. 165, 1195–1224.
Qiu, J.-T., Yu, X.-Q., Santosh, M., Zhang, D.-H., Chen, S.-Q., Li, P.-J., 2013. Geochronology and magmatic oxygen fugacity of the Tongcun molybdenum deposit, northwest Zhejiang, SE China. Miner. Depos. 48, 545–556.
Quebral, R.D., Pubellier, M., Rangin, C., 1996. The onset of movement on the Philippine Fault in eastern Mindanao: a transition from a collision to a strike-slip environment. Tectonics 15, 713–726.
Rangin, C., Jolivet, L., Pubellier, M., 1990. A simple model for the tectonic evolution of Southeast Asia and Indonesian region for the past 43 My. Bull. Geol. Soc. France 8, 889–905.
Rangin, C., Le Pichon, X., Mazzotti, S., Pubellier, M., Chamotrooke, N., Aurelio, M., Walpersdorf, A., Quebral, R., 1999. Plate convergence measured by GPS across the Sundaland/Philippine sea plate deformed boundary: the Philippines and eastern Indonesia. Geophys. J. Int. 139, 296–316.
Rapp, R.P., Shimizu, N., Norman, M.D., Applegate, G.S., 1999. Reaction between slab-derived melts and peridotite in the mantle wedge: experimental constraints at 3.8 GPa. Chem. Geol. 160, 335–356.
Reich, M., Parada, M.A., Palacios, C., Dietrich, A., Schultz, F., Lehmann, B., 2003. Adakite-like signature of Late Miocene intrusions at the Los Pelambres giant porphyry copper deposit in the Andes of central Chile: metallogenic implications. Miner. Depos. 38, 876–885.
Richards, J.P., 2011. High Sr/Y arc magmas and porphyry Cu±Mo±Au deposits: just add water. Econ. Geol. 106, 1075–1081.
Richards, J.P., Kerrich, R., 2007. Adakite-like rocks: their diverse origins and questionable role in metallogenesis. Econ. Geol. 102, 537–576.
Rudnick, R., Gao, S., 2003. Composition of the continental crust. Treatise Geochem. 3, 1–64.
Sajona, F.G., Maury, R.C., 1998. Association of adakites with gold and copper mineralization in the Philippines. Compt. Rend. Acad. Sci. Ser. Fasc. Sci. Terre Et Des Planet. 326, 27–34.
Sajona, F.G., Maury, R.C., Bellon, H., Cotten, J., Defant, M.J., Pubellier, M., 1993. Initiation of subduction and the generation of slab melts in western and eastern Mindanao, Philippines. Geology 21, 1007–1010.
Sajona, F.G., Maury, R.C., Bellon, H., Cotten, J., Defant, M., 1996. High field strength element enrichment of Pliocene-Pleistocene Island arc basalts, Zamboanga Peninsula, western Mindanao (Philippines). J. Petrol. 37, 693–726.
Sajona, F.G., Maury, R.C., Prouteau, G., Cotten, J., Schiano, P., Bellon, H., Fontaine, L., 2000a. Slab melt as metasomatic agent in island arc magma mantle sources, Negros and Batan (Philippines). Island Arc 9, 472–486.
Sajona, F.G., Maury, R.C., Pubellier, M., Leterrier, J., Bellon, H., Cotten, J., 2000b. Magmatic source enrichment by slab-derived melts in a young post-collision setting, central Mindanao (Philippines). Lithos 54, 173–206.
Schellart, W.P., Lister, G.S., Toy, V.G., 2006. A Late Cretaceous and Cenozoic reconstruction of the Southwest Pacific region: tectonics controlled by subduction and slab rollback processes. Earth Sci. Rev. 76, 191–233.
Schiano, P., Clocchiatti, R., Shimizu, N., Maury, R., Jochum, K., Hofmann, A., 1995. Hydrous, silica-rich melts in the sub-arc mantle and their relationship with erupted arc lavas. Nature 377, 595–600.
Schmidt, M.W., Dardon, A., Chazot, G., Vannucci, R., 2004. The dependence of Nb and Ta rutile–melt partitioning on melt composition and Nb/Ta fractionation during subduction processes. Earth Planet. Sci. Lett. 226, 415–432.
Sen, C., Dunn, T., 1994. Dehydration melting of a basaltic composition amphibolite at 1.5 and 2.0 GPa: implications for the origin of adakites. Contrib. Miner. Petrol. 117, 394–409.
Sillitoe, R.H., 2010. Porphyry copper systems. Econ. Geol. 105, 3–41.
Söderlund, U., Patchett, P.J., Vervoort, J.D., Isachsen, C.E., 2004. The 176Lu decay constant determined by Lu–Hf and U-Pb isotope systematics of Precambrian mafic intrusions. Earth Planet. Sci. Lett. 219, 311–324.
Stern, C.R., Kilian, R., 1996. Role of the subducted slab, mantle wedge and continental crust in the generation of adakites from the Andean Austral volcanic zone. Contrib. Miner. Petrol. 123, 263–281.
Sun, W.D., 2016. Initiation and evolution of the South China Sea: an overview. Acta Geochim. 35, 215–225.
Sun, S.S., McDonough, W.F., 1989. Chemical and isotopic systematics of oceanic basalts; implications for mantle composition and processes. In: Saunders, A.D., Norry, M.J. (Eds.), Magmatism in the Ocean Basins. Geological Society of London, London, United Kingdom, pp. 313–345.
Sun, W.D., Bennett, V.C., Eggins, S.M., Arculus, R.J., Perfit, M.R., 2003. Rhenium systematics in submarine MORB and back-arc basin glasses: laser ablation ICP-MS results. Chem. Geol. 196, 259–281.
Sun, W.D., Arculus, R.J., Kamenetsky, V.S., Binns, R.A., 2004. Release of gold-bearing fluids in convergent margin magmas prompted by magnetite crystallization. Nature 431, 975–978.
Sun, W.D., Ling, M.X., Yang, X.Y., Fan, W.M., Ding, X., Liang, H.Y., 2010. Ridge subduction and porphyry copper-gold mineralization: an overview. Sci. China Earth Sci. 53, 475–484.
Sun, W.D., Zhang, H., Ling, M.X., Ding, X., Chung, S.L., Zhou, J.B., Yang, X.Y., Fan, W.M., 2011. The genetic association of adakites and Cu–Au ore deposits. Int. Geol. Rev. 53, 691–703.
Sun, W.D., Ling, M.X., Chung, S.L., Ding, X., Yang, X.Y., Liang, H.Y., Fan, W.M., Goldfarb, R., Yin, Q.Z., 2012. Geochemical constraints on adakites of different origins and copper mineralization. J. Geol. 120, 105–120.
Sun, W.D., Liang, H.Y., Ling, M.X., Zhan, M.Z., Ding, X., Zhang, H., Yang, X.Y., Li, Y.L., Ireland, T.R., Wei, Q.R., Fan, W.M., 2013. The link between reduced porphyry copper deposits and oxidized magmas. Geochim. Cosmochim. Acta 103, 263–275.
Sun, W., Huang, R.-F., Li, H., Hu, Y.-B., Zhang, C.-C., Sun, S.-J., Zhang, L.-P., Ding, X., Li, C.-Y., Zartman, R.E., 2015. Porphyry deposits and oxidized magmas. Ore Geol. Rev. 65, 97–131.
Sun, W.-D., Li, C.-Y., Hao, X.-L., Ling, M.-X., Ireland, T., Ding, X., Fan, W.-M., 2016. Oceanic anoxic events, subduction style and molybdenum mineralization. Solid Earth Sci. 1, 64–73.
Sun, W., Wang, J.-T., Zhang, L.-P., Zhang, C.-C., Li, H., Ling, M.-X., Ding, X., Li, C.-Y., Liang, H.-Y., 2017. The formation of porphyry copper deposits. Acta Geochim. 36, 9–15.
Tamayo, R.A., Yumul, G.P., Maury, R.C., Polve, M., Cotten, J., Bohn, M., 2001. Petrochemical investigation of the Antique ophiolite (Philippines): implications on volcanogenic massive sulfide and podiform chromitite deposits. Resour. Geol. 51, 145–164.
Tatsumi, Y., 2006. High-Mg andesites in the Setouchi volcanic belt, southwestern Japan: analogy to Archean magmatism and continental crust formation? Annu. Rev. Earth Planet. Sci. 34, 467–499.
Thieblemont, D., Stein, G., Lescuyer, J.L., 1997. Epithermal and porphyry deposits: the adakite connection. Compt. Rend. Acad. Sci. Ser. Fasc. Sci. Terre Et Des Planet. 325, 103–109.
Thorkelson, D.J., 1996. Subduction of diverging plates and the principles of slab window formation. Tectonophysics 255, 47–63.
Thorkelson, D.J., Breitsprecher, K., 2005. Partial melting of slab window margins: genesis of adakitic and non-adakitic magmas. Lithos 79, 25–41.

Trail, D., Watson, E.B., Tailby, N.D., 2011. The oxidation state of Hadean magmas and implications for early Earth's atmosphere. Nature 480, 79–82.
Veevers, J.J., 2000. Change of tectono-stratigraphic regime in the Australian plate during the 99 Ma (mid-Cretaceous) and 43 Ma (mid-Eocene) swerves of the Pacific. Geology 28, 47–50.
Walia, M., Knittel, U., Suzuki, S., Chung, S.L., Pena, R.E., Yang, T.F., 2012. No Paleozoic metamorphics in Palawan (the Philippines)? Evidence from single grain U-Pb dating of detrital zircons. J. Asian Earth Sci. 52, 134–145.
Walther, H.W., Forster, H., Harre, W., Kreuzer, H., Lenz, H., Muller, P., Raschka, H., 1981. Early Cretaceous porphyry copper mineralization on Cebu Island, Philippines, dated with K-Ar and Rb-Sr methods. Geologisches Jahrbuch Reihe D 48, 21–35.
Wang, Q., Wyman, D.A., Xu, J., Jian, P., Zhao, Z., Li, C., Xu, W., Ma, J., He, B., 2007. Early Cretaceous adakitic granites in the Northern Dabie Complex, central China: implications for partial melting and delamination of thickened lower crust. Geochim. Cosmochim. Acta 71, 2609–2636.
Wang, F.Y., Liu, S.A., Li, S.G., He, Y.S., 2013. Contrasting zircon Hf-O isotopes and trace elements between ore-bearing and ore-barrenadakitic rocks in central-eastern China: implications for genetic relation to Cu-Au mineralization. Lithos 156–159, 97–111.
Wang, F.Y., Liu, S.A., Li, S.G., Akhtar, S., He, Y.S., 2014. Zircon U-Pb ages, Hf–O isotopes and trace elements of Mesozoic high Sr/Y porphyries from Ningzhen, eastern China: constraints on their petrogenesis, tectonic implications and Cu mineralization. Lithos 200–201, 299–316.
Wei, G.J., Liang, X.R., Li, X.H., Liu, Y., 2002. Precise measurement of Sr isotopic composition of liquid and solid base using (LP) MC-ICPMS. Geochimica 31, 295–305 (in Chinese with English abstract).
Winchester, J.A., Floyd, P.A., 1977. Geochemical discrimination of different magma series and their differentiation products using immobile elements. Chem. Geol. 20, 325–343.
Wong, J., Sun, M., Xing, G., Li, X.-H., Zhao, G., Wong, K., Yuan, C., Xia, X., Li, L., Wu, F., 2009. Geochemical and zircon U-Pb and Hf isotopic study of the Baijuhuajian metaluminous A-type granite: extension at 125–100 Ma and its tectonic significance for South China. Lithos 112, 289–305.
Wu, F.Y., Yang, Y.H., Xie, L.W., Yang, J.H., Xu, P., 2006. Hf isotopic compositions of the standard zircons and baddeleyites used in U-Pb geochronology. Chem. Geol. 234, 105–126.
Xiong, X.L., Adam, J., Green, T.H., 2005. Rutile stability and rutile/melt HFSE partitioning during partial melting of hydrous basalt: implications for TTG genesis. Chem. Geol. 218, 339–359.
Yogodzinski, G.M., Kay, R.W., Volynets, O.N., Koloskov, A.V., Kay, S.M., 1995. Magnesian andesite in the western Aleutian Komandorsky region: implications for slab melting and processes in the mantle wedge. Geol. Soc. Am. Bull. 107, 505–519.
Yogodzinski, G.M., Lees, J.M., Churikova, T.G., Dorendorf, F., Woerner, G., Volynets, O.N., 2001. Geochemical evidence for the melting of subducting oceanic lithosphere at plate edges. Nature 409, 500–504.
Yuan, H.L., Gao, S., Dai, M.N., Zong, C.L., Gunther, D., Fontaine, G.H., Liu, X.M., Diwu, C.R., 2008. Simultaneous determinations of U-Pb age, Hf isotopes and trace element compositions of zircon by excimer laser-ablation quadrupole and multiple-collector ICP-MS. Chem. Geol. 247, 100–118.
Yumul, G.P., 2007. Westward younging disposition of Philippine ophiolites and its implication for arc evolution. Island Arc 16, 306–317.
Yumul, G.P., Balce, G.R., Dimalanta, C.B., Datuin, R.T., 1997. Distribution, geochemistry and mineralization potentials of Philippine ophiolite and ophiolitic sequences. Ofioliti 22, 47–56.
Yumul, G.P., Dimalanta, C.B., Bellon, H., Faustino, D.V., De Jesus, J.V., Tamayo, R.A., Jumawan, F.T., 2000a. Adakitic lavas in the Central Luzon back-arc region, Philippines: lower crust partial melting products? Island Arc 9, 499–512.
Yumul, G.P., Dimalanta, C.B., Tamayo, R.A., Barretto, J.A.L., 2000b. Contrasting morphological trends of islands in Central Philippines: speculation on their origin. Island Arc 9, 627–637.
Yumul, G.P., Dimalanta, C.B., Tamayo, R.A., Bellon, H., 2003. Silicic arc volcanism in Central Luzon, the Philippines: characterization of its space, time and geochemical relationship. Island Arc 12, 207–218.
Yumul, G.P., Dimalanta, C.B., Maglambayan, V.B., Marquez, E.J., 2008. Tectonic setting of a composite terrane: a review of the Philippine island are system. Geosci. J. 12, 7–17.
Yumul, G.P., Brown, W.W., Dimalanta, C.B., Ausa, C.A., Faustino-Eslava, D.V., Payot, B.D., Ramos, N.T., Lizada, A.N.L., Buena, A.E., Villaplaza, B.R.B., 2016. Adakitic rocks in the Masara gold-silver mine, Compostela Valley, Mindanao, Philippines: different places, varying mechanisms? J. Asian Earth Sci. http://dx.doi.org/10.1016/j.jseaes.2016.1006.1005.
Zhan, M.Z., Sun, W.D., Ling, M.X., Li, H., 2015. Huangyan ridge subduction and formation of porphyry Cu–Au deposits in Luzon. Acta Petrol. Sin. 31, 2101–2114.
Zhang, Q., Qin, K.Z., Wang, Y., Zhang, F.Q., Liu, H.T., Wang, Y., 2004. Study on adakite broadened to challenge the Cu and Au exploration in China. Acta Petrol. Sin. 20, 195–204 (in Chinese with English abstract).
Zhang, H., Ling, M.-X., Liu, Y.-L., Tu, X.-L., Wang, F.-Y., Li, C.-Y., Liang, H.-Y., Yang, X.-Y., Arndt, N.T., Sun, W.-D., 2013. High oxygen fugacity and slab melting linked to Cu Mineralization: evidence from dexing porphyry copper deposits, Southeastern China. J. Geol. 121, 289–305.
Zhang, C.-C., Sun, W.-D., Wang, J.-T., Zhang, L.-P., Sun, S.-J., Wu, K., 2017a. Oxygen fugacity and porphyry mineralization: a zircon perspective of Dexing porphyry Cu deposit, China. Geochim. Cosmochim. Acta 206, 343–363.
Zhang, L., Hu, Y., Liang, J., Ireland, T., Chen, Y., Zhang, R., Sun, S., Sun, W., 2017b. Adakitic rocks associated with the Shilu copper–molybdenum deposit in the Yangchun Basin, South China, and their tectonic implications. Acta Geochim., 1–19
Zhou, D., Sun, Z., Chen, H.Z., Xu, H.H., Wang, W.Y., Pang, X., Cai, D.S., Hu, D.K., 2008. Mesozoic paleogeography and tectonic evolution of South China Sea and adjacent areas in the context of Tethyan and Paleo-Pacific interconnections. Island Arc 17, 186–207.